J. Fluid Mech. (2007), *vol.* 580, *pp.* 219–249.
doi:10.1017/S0022112007005228 Printed in the United Kingdom

Theory of vaporization of a rigid spherical droplet in slowly varying rectilinear flow at low Reynolds numbers

G. DEL ÁLAMO AND F. A. WILLIAMS

Center for Energy Research, Department of Mechanical and Aerospace Engineering, University of California San Diego, La Jolla, CA, 92093-0411, USA

(Received 15 June 2006 and in revised form 4 December 2006)

The vaporization of a droplet in rectilinear motion relative to a stagnant gaseous atmosphere is addressed for the limit of low Reynolds numbers and slow variation of the droplet velocity. Approximations are introduced that enable a formal asymptotic analysis to be performed with a minimum of complexity. It is shown that, under the conditions addressed, there is an inner region in the vicinity of the droplet within which the flow is nearly quasi-steady except during short periods of time when the acceleration changes abruptly, and there is a fully time-dependent outer region in which departures of velocities and temperatures from those of the ambient medium are small. Matched asymptotic expansions, followed by a Green's function analysis of the outer region enable expressions to be obtained for the velocity and temperature fields and for the droplet drag and vaporization rate. The results are applied to problems in which the droplet experiences constant acceleration, constant deceleration and oscillatory motion. The results, which identify dependences on the Prandtl number and the transfer number, are intended to be compared with experimental measurements on droplet behaviours in time-varying flows.

1. Introduction

Because of interest in understanding spray-combustion characteristics in rocket and gas-turbine combustors, internal combustion engines and oil-fired furnaces, studies of the combustion of fuel droplets have remained active research topics for over fifty years. Godsave (1953) and Spalding (1953) were the first to offer simplified models for the spherically symmetrical combustion of a liquid fuel droplet in a gaseous oxidizing atmosphere, envisioning the combustion to be diffusion-controlled and thereby deriving the well-known d-square law, according to which the square of the droplet diameter decreases linearly with time. Numerous reviews of this work and somewhat later developments have been written, among them Williams (1965), Williams (1973), Faeth (1977) and Law (1982). Most investigations pertain to quasi-steady conditions, an approximation justifed for stationary droplets by the typically large ratio of liquid to gas density at normal atmospheric conditions, and some authors (Fendell, Sprankle & Dodson 1966; Fendell 1968; Gogos *et al.* 1986; Wichman & Baum 1993; Jog, Ayyaswamy & Cohen 1996; Ackerman & Williams 2005) address non-spherical quasi-steady convection in droplet combustion for small Reynolds numbers under these conditions. For large ratios of liquid to gas densities there have been relatively few studies of the possible time-dependent effects, although Crespo & Liñán (1975) and Waldman (1975) analysed the time-dependent behaviour for

spherical symmetry. More recent reviews are available (see for example Sirignano 1983, 1999; Williams 1985; Dwyer 1989; Chiu 2000). The ultimate interest of the present study is to consider effects of non-spherical time-dependent convection on the combustion of droplets having a large ratio of liquid to gas density, since in many applications the velocity of the droplet relative to the gas varies with time under such conditions.

To approach this problem, attention here is focused on vaporization of a droplet in slowly varying flows at low Reynolds numbers. Conditions are addressed in which the gas density can be approximated as being constant, that is, large temperature changes are excluded. Although this approximation is unrealistic in droplet-combustion applications, a thorough understanding of the constant-density problem is required before variable-density effects can be addressed properly, and through judicious selection of values of properties, it has in fact been possible to relate results of constant-density analysis to results of droplet-combustion experiments in the presence of slow forced convection (Ackerman & Williams 2005). To enable asymptotic analysis to be pursued as clearly and simply as possible, a number of other simplifying assumptions will be involved, greatly reducing the number of parameters that otherwise would appear, so that many different spray-combustion and droplet-combustion effects, discussed in the previously cited literature and of importance under various circumstances, are not addressed.

Given the approximations of a constant gas density and a large ratio of liquid to gas density, significant literature that does not address combustion underlies the present investigation (Fuchs 1959). The latter approximation enables the time variation of the droplet diameter to be neglected, as is done here. The problem then reduces to that of determining the velocity and temperature fields for flow around a sphere of fixed diameter. That flow, in general, induces flow of the liquid inside the droplet (Levich 1962; Sadhal & Ayyaswamy 1983), but in the present work, to minimize the number of parameters that appear in the problem so as to simplify the results and facilitate understanding, it is assumed that the liquid viscosity is sufficiently large for liquid motion to be neglected (often a reasonable approximation). Therefore only rigid spherical droplets are addressed. Moreover, for similar reasons, temperature variations within the liquid are neglected, so that only gas-phase conservation equations need be addressed. Boundary conditions at the droplet surface lead to specification of the temperature there as the vaporization temperature, determination of the proportionality between the heat flux to the droplet surface and the vaporization rate through the transfer number (denoted by B and defined below), and imposition of the no-slip condition for the velocity field there.

The droplet vaporization results in radially outward flow at the droplet surface, which then interacts with the externally imposed non-spherical convection through the equations of mass and momentum conservation. Consideration of this interaction distinguishes the present investigation from many previous investigations in which flow through the surface of the sphere is neglected. In that limit of a neglegible mass source, in the first approximation for low Reynolds numbers in steady flow, the Stokes drag law applies (Stokes 1851), the uniformly valid leading-order flow field having been first obtained by Oseen (1910), as explained by Proudman & Pearson (1957). Heat and mass transfer in this same mass-source-free type of steady flow, leading to determination of Nusselt numbers, were addressed somewhat later (Acrivos & Taylor 1962; Brenner 1963; Batchelor 1979), and the effect of the mass source on the flow was considered subsequently (Sadhal & Ayyaswamy 1983; Chung, Ayyaswamy & Sadhal 1984). With coupling between the heat-transfer rate and the strength of the

mass source, bringing in the equation for energy conservation, the Prandtl number σ becomes an additional parameter in the problem addressed here. A number of results will be summarized for steady flow, in forms simpler than those that can be found in the literature.

Time-varying motions of droplets can introduce numerous complications that depend strongly on the type of motion (Clift, Grace & Weber 1978). For this reason, if analytical progress is to be made, it is necessary to restrict attention to particular classes of motion. With this in mind, only straight-line rectilinear motion is considered here, as a first step that must be undertaken before it is reasonable to address other more complex motions. Moreover, to enable expansions to be developed, attention is restricted to slowly varying conditions, for which the flow in the vicinity of the droplet is quasi-steady in the first approximation. The unsteady force on solid spheres in flows of this type has been considered previously (Ockendon 1968; Sano 1981; Hinch 1993; Asmolov 2001), and heat transfer to spheres in such flows has been analysed without considering mass-source effects (Choudhury & Drake 1971; Abramzon & Elata 1984; Feng & Michaelides 1996; Pozrikidis 1997). These various studies have addressed acceleration, deceleration and oscillatory motion, but not coupling of the momentum and energy fields, which is the subject of the present work. The Greens-function methods of previous studies (Pozrikidis 1997), however, are essential in the present analysis, which addresses diffusion-controlled droplet evaporation in the limit of low-velocity flow varying slowly in time.

2. Statement of the problem

A theoretical analysis employing matched asymptotic expansions is presented. For a droplet of diameter d, in a flow with a characteristic external velocity u_e measured with respect to the droplet, a characteristic Reynolds number based on droplet radius is

$$\epsilon = \frac{du_e}{2\nu}, \tag{2.1}$$

where ν denotes the kinematic viscosity. Since attention is focused on small Reynolds numbers, ϵ will be a small parameter of expansion. For small ϵ there are two distinguished regions in the flow, an inner Stokes region where the radius is of order d and an outer Oseen region where the radius is of order d/ϵ. A characteristic diffusion time in the Oseen region is therefore $t_o = d^2/4\nu\epsilon^2$, and the ratio of this to a characteristic time t_e of variation of the external velocity is

$$c = t_o/t_e = \frac{d^2}{4\nu\epsilon^2 t_e}. \tag{2.2}$$

The analysis to be developed treats c of order unity and ϵ as a small parameter.

The ratio of a characteristic diffusive time in the Stokes region, $t_s = d^2/4\nu$, to the characteristic time t_e is $c\epsilon^2$ according to (2.2), which is very small for small ϵ and c of order unity. This favours applicability of quasi-steady solutions in the Stokes region to leading order. Although the formulation will allow for general time variations of the external velocity under these restrictions, specific problems resulting in somewhat special expansions will be addressed. One is the acceleration of the droplet from rest in a stagnant atmosphere at a constant acceleration a. In this case, there is no imposed characteristic velocity u_e, and since the Oseen region is expected to control the characteristic evolution time for c of order unity, the value of c in (2.2) may be set

equal to unity, resulting, with the definition $t_e = u_e/a$ and with (2.1), in the expression

$$\epsilon = \frac{da^{1/3}}{2\nu^{2/3}} \tag{2.3}$$

for the small parameter of expansion; this corresponds to $u_e = (a\nu)^{1/3}$, making the convection and diffusion terms in the Oseen region of the same order of magnitude. Another problem concerns the deceleration of a droplet initially vaporizing quasi-steadily in a flow of constant external velocity u_e, with a constant deceleration rate a imposed after time zero. In this case, (2.1) defines the relevant Reynolds number ϵ, and (2.2) again applies for c with $t_e = u_e/a$. In a general situation, the maximum imposed external velocity would be used to define the small parameter ϵ, and the maximum absolute value of the acceleration would be used to define the parameter c.

The last problem to be addressed in this work corresponds to the evaporation of a droplet in sinusoidal oscillatory motion about a mean velocity u_e, with constant frequency ϖ and amplitude of the oscillations u'_e. In this case, (2.1) and (2.2) are used to define ϵ and c, with $t_e = \varpi^{-1}$ being the appropriate characteristic time of variation of the external velocity. For purely oscillatory motion with zero mean velocity, the amplitude of the oscillation is taken to be the characteristic external velocity, and therefore $\epsilon = du'_e/(2\nu)$ becomes the corresponding Reynolds number.

3. Formulation

The problem is formulated initially with non-dimensional variables appropriate for the Stokes region. The droplet radius $d/2$ and the diffusion time in the Stokes region $d^2/4\nu$ are chosen as scales for length and time, and the viscous velocity $2\nu/d$ is selected as the scale for velocity. For simplicity, the density, specific heat, thermal conductivity and coefficient of viscosity are assumed constant, and the conservation equations are written in a coordinate system attached to the droplet. This is an inertial system when the droplet is stationary and the fluid is moving or if the droplet is moving at constant velocity in an ambient fluid at rest, but it is a non-inertial system if the droplet moves at variable velocity. Because of the constant-density approximation, both situations can be described by the same formulation if an additional acceleration term is included in the body force, making an additional contribution to the hydrostatic pressure gradient when the droplet is in variable motion. With p' denoting the resulting non-dimensional ratio of pressure to density (non-dimensionalized by the square of the viscous velocity), $\boldsymbol{\tau}'$ denoting the corresponding non-dimensional viscous stress tensor and $\boldsymbol{g}'$ the non-dimensional acceleration by body forces, the mass, momentum and energy conservation equations become

$$\nabla \cdot (\boldsymbol{v}) = 0, \tag{3.1}$$

$$\frac{\partial \boldsymbol{v}}{\partial t} + \boldsymbol{v} \cdot \nabla \boldsymbol{v} = -\nabla p' + \boldsymbol{g}' + \nabla \cdot \boldsymbol{\tau}' \tag{3.2}$$

and

$$\frac{\partial \theta}{\partial t} + \boldsymbol{v} \cdot \nabla \theta = \frac{\nabla^2 \theta}{\sigma}. \tag{3.3}$$

Here σ is the Prandtl number, $\boldsymbol{v}$ denotes the non-dimensional velocity vector, and the non-dimensional temperature is

$$\theta = (T - T_s)/(T_\infty - T_s), \tag{3.4}$$

where T denotes temperature, the subsript s identifies conditions at the surface of the droplet, and the subscript ∞ denotes conditions in the ambient gas.

In the far field, the boundary conditions at infinity are

$$\theta = 1, \qquad \boldsymbol{v} = \epsilon U \boldsymbol{e}_x, \tag{3.5}$$

where U represents the ratio of the instantaneous external velocity (with respect to the droplet) to u_e, so that ϵU is the instantaneous Reynolds number, and the x-direction has been taken to be the direction of the external velocity (assumed not to change with time), $\boldsymbol{e}_x$ denoting a unit vector in the x-direction. The non-dimensional radial coordinate will be denoted by r, and at the droplet surface ($r = 1$), the tangential component of velocity must vanish because of the no-slip condition, the liquid being assumed sufficiently viscous to prevent internal fluid motion. The heat of vaporization per unit mass for the liquid L_v is assumed to be large compared to the product of the gas constant per unit mass for the vapour and the boiling temperature, whence from the Clausius–Claperyon relation, the temperature at the droplet surface T_s becomes approximately constant and equal to the boiling temperature. The other boundary conditions at the droplet surface become

$$\theta = 0, \qquad \frac{\partial \theta}{\partial r} = \frac{\sigma}{B} v_r, \qquad v_r = b, \tag{3.6}$$

where the transfer number, to be taken as of order unity, is $B = c_p(T_\infty - T_s)/L_v$, c_p denoting the specific heat at constant pressure, v_r is the radial component of the non-dimensional velocity, and the non-dimensional radial velocity b in the gas at the droplet surface depends in general on both time and the polar angle $\cos^{-1}\mu$ measured from the direction of the external gas velocity (the x-axis). By symmetry, the velocity and temperature fields are axisymmetric, independent of the azimuthal coordinate in a spherical polar coordinate system.

It is convenient to introduce a non-dimensional streamfunction ψ, replacing the momentum conservation equation by a vorticity conservation equation, and to write the resulting conservation equations explicitly in terms of t, the non-dimensional radial coordinate r and the independent variable μ, the cosine of the polar angle. Equations (3.1), (3.2) and (3.3) then reduce to

$$\mathrm{D}^4\psi + L(\psi, \mathrm{D}^2\psi) = \frac{\partial}{\partial t}\mathrm{D}^2\psi \tag{3.7}$$

and

$$\nabla^2\theta + C(\psi, \theta) = \sigma \frac{\partial \theta}{\partial t}, \tag{3.8}$$

where

$$\mathrm{D}^2 = \frac{\partial^2}{\partial r^2} + \frac{1-\mu^2}{r^2}\frac{\partial^2}{\partial \mu^2}, \tag{3.9}$$

$$\nabla^2 = \frac{1}{r^2}\frac{\partial}{\partial r}\left(r^2 \frac{\partial}{\partial r}\right) + \frac{1}{r^2}\frac{\partial}{\partial \mu}\left((1-\mu^2)\frac{\partial}{\partial \mu}\right), \tag{3.10}$$

$$L(\psi, \mathrm{D}^2\psi) = \frac{1}{r^2}\left[\frac{\partial \psi}{\partial \mu}\frac{\partial}{\partial r}\mathrm{D}^2\psi - \frac{\partial \psi}{\partial r}\frac{\partial}{\partial \mu}\mathrm{D}^2\psi - 2\frac{\partial \psi}{\partial r}\frac{\mu}{1-\mu^2}\mathrm{D}^2\psi - \frac{2}{r}\frac{\partial \psi}{\partial \mu}\mathrm{D}^2\psi\right] \tag{3.11}$$

and

$$C(\psi, \theta) = \frac{\sigma}{r^2}\left(\frac{\partial \psi}{\partial \mu}\frac{\partial \theta}{\partial r} - \frac{\partial \psi}{\partial r}\frac{\partial \theta}{\partial \mu}\right). \tag{3.12}$$

Equations (3.7) and (3.8) are to be solved subject to the boundary conditions

$$\frac{\partial\psi}{\partial r}=0, \qquad \frac{\partial\psi}{\partial\mu}=-b, \qquad \theta=0, \qquad \frac{\partial\theta}{\partial r}=\frac{\sigma b}{B} \tag{3.13}$$

at $r=1$ and

$$\psi=\tfrac{1}{2}\epsilon U r^2(1-\mu^2), \qquad \theta=1 \tag{3.14}$$

at $r=\infty$, and initial conditions $\psi_i(r,\mu)$ and $\theta_i(r,\mu)$. It is assumed that prior to the onset of variation of the external velocity, the droplet is evaporating steadily and possibly moving steadily. Uniformly valid matched asymptotic expansions of the solutions ψ and θ based on the small parameter ϵ will be sought. The non-dimensional vaporization velocity b at the droplet surface is to be determined in the course of the solution, the non-dimensional total vaporization rate, $M=2\pi\int_{-1}^{1} b\,\mathrm{d}\mu$, being of particular interest.

4. The inner problem and the quasi-steady inner solution

In the Stokes region, the solutions for ψ, θ and b can be written for small ϵ in terms of the expansions

$$\psi=\psi_0+\epsilon\psi', \qquad \theta=\theta_0+\epsilon\theta', \qquad b=b_0+\epsilon b', \tag{4.1}$$

where the leading-order terms

$$\psi_0=-\mu b_0, \qquad \theta_0=\frac{1}{B}\left\{(1+B)^{1-1/r}-1\right\}, \qquad b_0=\frac{\ln(1+B)}{\sigma} \tag{4.2}$$

correspond to steady vaporization of a droplet at rest in a stagnant atmosphere. The first perturbations ψ' and θ' are then found from (3.7) and (3.8) to obey

$$\mathrm{D}^4\psi'+\epsilon L(\psi',\mathrm{D}^2\psi')-\frac{b_0}{r^2}\left(\frac{\partial}{\partial r}-\frac{2}{r}\right)\mathrm{D}^2\psi'=\frac{\partial}{\partial t}\mathrm{D}^2\psi', \tag{4.3}$$

and

$$\nabla^2\theta'+\epsilon C(\psi',\theta')-\frac{\sigma b_0}{r^2}\frac{\partial\theta'}{\partial r}+\frac{\sigma b_0(1+B)^{1-1/r}}{Br^4}\frac{\partial\psi'}{\partial\mu}=\sigma\frac{\partial\theta'}{\partial t}, \tag{4.4}$$

with boundary conditions

$$\frac{\partial\psi'}{\partial r}=0, \qquad \frac{\partial\psi'}{\partial\mu}=-b', \qquad \theta'=0, \qquad \frac{\partial\theta'}{\partial r}=\frac{\sigma b'}{B} \tag{4.5}$$

at $r=1$, obtained from (3.13), and matching conditions with the outer solution at $r\to\infty$.

By introducing Gegenbauer polynomials for the angular dependence of ψ' and Legendre polynomials for the angular dependences of θ' and b', the solutions to (4.3)–(4.5) can be written as

$$\psi'=U\left\{-\mu\lambda+\tfrac{1}{2}(1-\mu^2)f\right\}, \qquad \theta'=\sigma U\{g-\mu h\}, \qquad b'=U\{\lambda-\mu\chi\}, \tag{4.6}$$

where the functions $f(r,t)$, $g(r,t)$ and $h(r,t)$ as well as $\lambda(t)$ and $\chi(t)$ remain to be obtained. For large t, a quasi-steady solution to (3.7)–(3.8) applies in the first approximation for small ϵ. The resulting quasi-steady problem has been treated extensively in the literature (Fendell 1968; Sadhal & Ayyaswamy 1983; Chung, Ayyaswamy & Sadhal 1984), and it can be shown that, neglecting terms of higher order in ϵ,

$$\lambda=g_\infty B/(1+B) \tag{4.7}$$

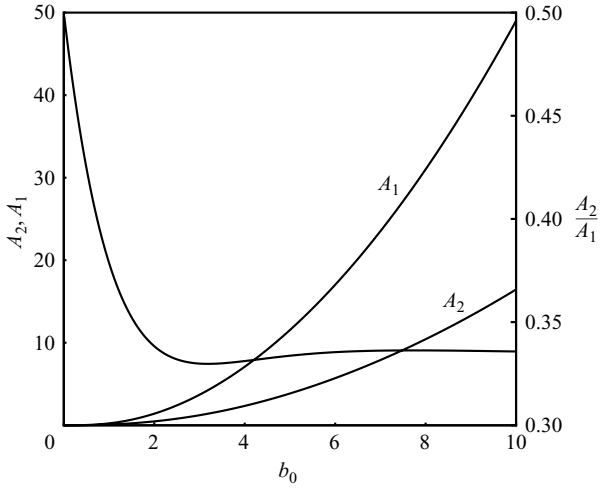

FIGURE 1. Variations of the constants A_1 and A_2 given by (4.9) and (4.10) and of the ratio A_2/A_1 with the unperturbed non-dimensional vaporization rate b_0.

and

$$\chi = \frac{1 - K_1 - (1 - 3A_2/A_1)K_3 - 3K_4/A_1}{K_2 + (1 - A_2/A_1)K_3 + K_4/A_1}, \tag{4.8}$$

where

$$A_1 = b_0^2/2 - 1 + (1 + b_0)\,\mathrm{e}^{-b_0} \tag{4.9}$$

and

$$A_2 = b_0^2/6 - 1/5 - \left[\left(b_0^4 - b_0^3 + 2b_0^2 - 6b_0 - 6\right)/30\right]\mathrm{e}^{-b_0}, \tag{4.10}$$

which are plotted in figure 1, and K_1, K_2, K_3 and K_4 are given in Appendix A, while

$$f = r^2 + \frac{2}{r} - \frac{3 + \chi}{r}\left\{1 + \frac{b_0^5}{A_1}\left[\int_{1/b_0}^{r/b_0} (\xi^3 + \xi^4)\,\mathrm{e}^{-1/\xi}\,\mathrm{d}\xi + \frac{r^3 - 1}{6b_0^3} - \frac{r^5 - 1}{5b_0^5}\right]\right\}, \tag{4.11}$$

$$g = g_\infty (1 - 1/r)(1 + B)^{-1/r} \tag{4.12}$$

and

$$h = [C\,\mathrm{e}^{-\sigma b_0} + V_2(r)]\left(1 - \frac{2r}{\sigma b_0}\right) - \left[C\left(\frac{2 - \sigma b_0}{2 + \sigma b_0}\right) + V_1(r)\right]\left(1 + \frac{2r}{\sigma b_0}\right)\mathrm{e}^{-\sigma b_0/r}, \tag{4.13}$$

where the functions $V_1(r)$ and $V_2(r)$ are defined as

$$V_1 = \frac{1 + B}{B}\int_1^r \left(1 - \frac{2r}{\sigma b_0}\right)\frac{f(r)}{r^2}\,\mathrm{d}r \tag{4.14}$$

and

$$V_2 = \frac{1 + B}{B}\int_1^r \left(1 + \frac{2r}{\sigma b_0}\right)\frac{f(r)}{r^2}\,\mathrm{e}^{-\sigma b_0/r}\,\mathrm{d}r, \tag{4.15}$$

and

$$C = \frac{(1 + B)(2 + \sigma b_0)}{B(\sigma b_0)^2 K_2}\{1 - K_1 + 2K_3 - (3 + \chi)[K_3(1 - A_2/A_1) + K_4/A_1]\}. \tag{4.16}$$

Expansions of χ, f, g and h for small and large values of b_0 are given in Appendix B.

These results are stated here, without derivation, in what appears to be an optimally compact form which cannot be found in the literature. It may be noted from these results that, even for the time-dependent problem, the functions f and h are independent of t, and χ is a constant. These functions and the constant χ are determined uniquely by just two parameters, the thermodynamic variable B and the transport property σ, the non-dimensional leading-order vaporization rate b_0 being related to these by (4.2). The angular dependences of the temperature field and vaporization rate are carried by the time-independent function h and eigenvalue χ, and these dependences average to zero when integrated over all angles. The time dependences of the vaporization rate and the temperature field appear only in U, λ and g and, given U, are determined by the single function $g_\infty(t)$, which must be obtained by matching. Except for the given function $U(t)$ and the simple dependence arising through $\lambda(t)$, the velocity field depends only on the function f, which is seen from (4.11) to be independent of t, like h and χ, and determined uniquely by b_0 and σ. The normalized non-dimensional vorticity in the inner region can be expressed as $\omega = -\epsilon\sqrt{1-\mu^2}\Omega/r$, with $\Omega = \mathrm{d}^2 f/\mathrm{d}r^2 - 2f/r^2$. Introducing the expression for f given by (4.11) into this formula for Ω gives

$$\Omega = \frac{2(3+\chi)r^2}{A_1}\left\{\mathrm{e}^{-b_0/r}\left(1+\frac{b_0}{r}+\frac{b_0^2}{2r^2}\right)-1\right\}, \tag{4.17}$$

the functional form of which depends only on b_0, the Prandtl number σ appearing only in the prefactor. The only unknown to be determined by matching to the outer region then, up to terms of order ϵ^2, is g_∞, which affects the temperature field and the vaporization rate.

5. Properties of the quasi-steady inner solution

5.1. *Velocity field and mass source*

From (4.1), (4.6) and (4.7), the non-dimensional vaporization velocity can be written, up to terms of order ϵ^2, as

$$b = b_0 + \epsilon U\{g_\infty B/(1+B) - \mu\chi\}, \tag{5.1}$$

in which U and g_∞ determine the time dependence and χ the angular dependence. Values of χ obtained from (4.8) are plotted in figure 2 as a function of b_0 for three values of σ. It can be seen that there is a monotonic increase of χ with b_0, which goes from zero at $b_0 = 0$ to

$$\chi_\infty = 15\sigma^3\left\{\sigma^5\ln\left(\frac{1+\sigma}{\sigma}\right) + (10\sigma^2+15\sigma+6)\ln(1+\sigma) - \sigma^4 + \frac{\sigma^3}{2} - 12\sigma^2 - 6\sigma\right\}^{-1} - 3, \tag{5.2}$$

at $b_0 = \infty$. The dependence of χ_∞ on the Prandtl number σ is shown in figure 3, which exhibits an increase of χ_∞ with σ from $3\sigma/2$ at small σ to $3\sigma/(2\ln\sigma)$ at large σ. Thus, in addition to increasing in proportion to the external relative velocity (through U) and to the apparent external temperature increase (through g_∞), the vaporization rate becomes larger in the upstream direction and smaller in the downstream direction, by an amount which increases with increasing unperturbed vaporization velocity and with increasing Prandtl number, lower thermal conductivities enhancing the angular dependence.

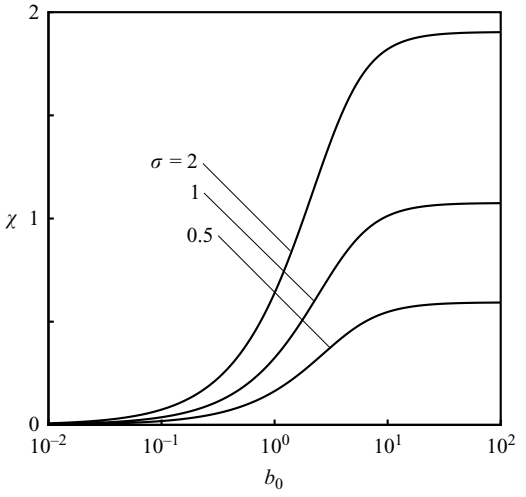

FIGURE 2. Variations of χ, the non-dimensional coefficient of the angular dependence of the vaporization rate, with the unperturbed non-dimensional vaporization rate b_0 evaluated from (4.8) for different values of the Prandtl number ($\sigma = 0.5$, 1 and 2).

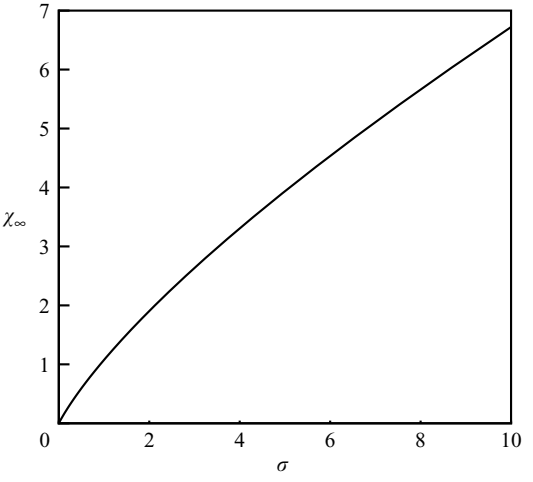

FIGURE 3. Dependence of χ_∞ on σ obtained from (5.2), showing how, in the limit of large vaporization rates, the strength of the angular dependence of the vaporization rate increases with the Prandtl number.

The non-dimensional total vaporization rate $M = 2\pi \int_{-1}^{1} b \, \mathrm{d}\mu$ can be calculated from the solution for b in (5.1) to give

$$M = 4\pi\{[\ln(1+B)]/\sigma + \epsilon U g_\infty B/(1+B)\}. \tag{5.3}$$

From (3.1), it can be shown that M is the total rate of mass transfer through any spherical surface in the inner zone surronding the droplet (and centred at the droplet centre) divided by the product of the viscosity coefficient and the droplet radius. Applying this result to large values of r demonstrates that sufficiently far from its surface the droplet behaves like a point source of mass, the strength of which increases with increasing B, U, g_∞ and thermal conductivity (through σ).

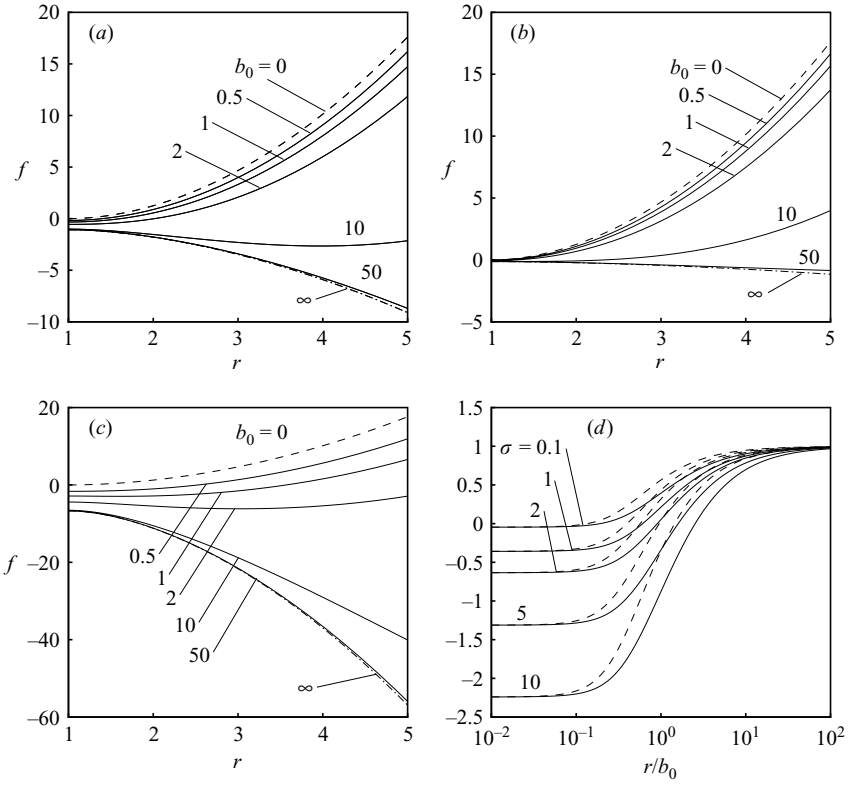

FIGURE 4. The rotational component of the velocity field in the inner region. (*a–c*) Variations with r of the component f of the non-dimensional perturbation streamfunction ψ' of (4.6), as given by (4.11), for various values of b_0 (solid lines: $b_0 = 0.5, 1, 2, 10$ and 50; dashed lines: $b_0 = 0$; dashed-dotted lines: $b_0 = \infty$) and for different values of Prandtl number ((*a*) $\sigma = 1$; (*b*) $\sigma = 0.1$; (*c*) $\sigma = 10$). (*d*) —, The radial and - - -, tangential components of the non-dimensional velocity, normalized by the product ϵU, in the strong-vaporization limit. $b_0 \gg 1$.

The velocity field, determined by the streamfunction, is purely radial and irrotational at leading order in the inner zone, and there is an additional irrotational radial contribution, through λ in (4.6), in the perturbation. In addition to that, the perturbation introduces a non-radial angular-dependent rotational contribution through f. The dependence of this component of the non-dimensional streamfunction on r for various values of b_0 is shown in figure 4, for three different values of σ. The corresponding radial and tangential components of the non-dimensional velocity, normalized by the product ϵU, are $\mu f/r^2$ and $-\sqrt{1-\mu^2}(\mathrm{d}f/\mathrm{d}r)/(2r)$, respectively, and they are plotted for the limit of large b_0 in figure 4(*d*). The rotational part of the velocity field generates an angular-dependent component in the distribution of the non-dimensional pressure p' of (3.2), which, normalized by the product ϵU, can be written as μp with

$$p = f'''/(2r) - [b_0 + 1/(2r^2)]f'' + f'[1/(2r^3) - 1/r^2] + 2f/r^3, \tag{5.4}$$

the prime here denoting differentiation with respect to r.

Figure 4 shows that at the droplet surface, the function f is negative with zero slope, except in the limit $b_0 = 0$, in which case the value is zero. In this limit, from the expansion given in Appendix B it is seen that $f = r^2 - 3r/2 + 1/(2r)$, which is

the non-dimensional streamfunction for a non-vaporizing sphere in steady flow for all values of σ, plotted as dashed curves in figure 4(*a–c*). The curves in figure 4 for small b_0 have positive curvature for all r, so f becomes positive near the droplet surface, at a radial distance that increases with increasing vaporization velocity. The curves for large b_0, however, have a negative curvature near the droplet surface, and f becomes positive only far from the surface. From the expansions for large b_0 given in Appendix B, it can be seen that near the droplet surface, where r is of order unity, the non-dimensional streamfunction approaches the negative-valued function $f = -(\chi_\infty/3)(r^2 + 2/r)$, for which the velocity field is irrotational; this is shown as the dot-dash curves in figure 4(*a–c*). Essentially, at large b_0, the vorticity region is blown away from the droplet surface, and a mixing region develops at large r, the flow being reversed on the droplet side, as will now be described more fully.

As shown in Appendix B, to investigate the blown-off mixing region it is appropriate to rescale r with b_0 and f with b_0^2. Figure 4(*d*) shows the resulting normalized non-dimensional radial and tangential velocity components from f in this rescaled mixing region. These perturbations become equal, implying a purely axial component of the velocity field, not only outside the mixing region but also on the droplet side of it. Moreover, on the droplet side the tangential velocity component points upstream, except when $\sigma = 0$, in which case it is zero. This reverse flow is generated by the interactions of the angular-dependent source flow with the externally imposed uniform flow. Expanding (5.4) for large b_0 gives $p/b_0 = f''$ at leading order in b_0^{-1}, indicating that the angular-dependent component of the pressure is given mainly by the momemtum flux in the tangential direction. Since the angular-dependent tangential velocity component points upstream, which it must do to satisfy continuity as a consequence of the relative increase of the vaporization rate on the upstream side of the droplet, the pressure gradient in the tangential direction, $\sqrt{1-\mu^2}\,p/r$, becomes negative, reversing the flow in this perturbation contribution. The pressure gradient, and consequently the strength of the reverse flow, increases with σ, smaller thermal conductivities favouring larger perturbations through the interactions. In figure 4(*d*) it is seen that, except at the edges of the mixing region, the tangential velocity component always lies above the radial velocity perturbations, that is, the shear is largely in the tangential direction.

To illustrate more clearly the structure of the inner solution in the large-b_0 limit, the perturbation streamlines and isotherms calculated from the large-b_0 inner solution of figure 4(*d*), for a droplet evaporating steadily in a constant-velocity flow are plotted in figure 5. The expressions for ψ' and θ used to obtained the curves in figure 5 are given by (4.1), (4.2) and (4.6)–(4.16) with $g_\infty = \sigma(1+B)/(2B)$, the value obtained from matching to the outer solution for steady flow. It can be seen in figure 5 that, for large b_0, the effect of higher Prandtl numbers is to increase the strength of the reverse flow and decrease the temperature of the inner region, the reverse-flow tendency being especially evident from the separation region downstream from the droplet, seen in figure 5(*b*). The separation region, with reverse flow present everywhere around the droplet, is, of course, present only in the perturbation, as may be seen, for example, from the streamlines for the full solution, obtained from (4.1), (4.2) and (4.6), plotted in figure 6 for $\epsilon U = 0.1$, with the other parameters corresponding to figure 5(*b*).

The different behaviour of the velocity field for strong vaporization, as compared with the behaviour for weak or moderate vaporization, may also be viewed in terms of the vorticity in the inner region. Figure 7 shows (for $\sigma = 1$) the r dependence of the vorticity factor Ω given by (4.17), for the values of b_0 that were selected for figure 4(*a*). For $b_0 = 0$, 0.5 and 1, at the droplet surface, the vorticity has a maximum

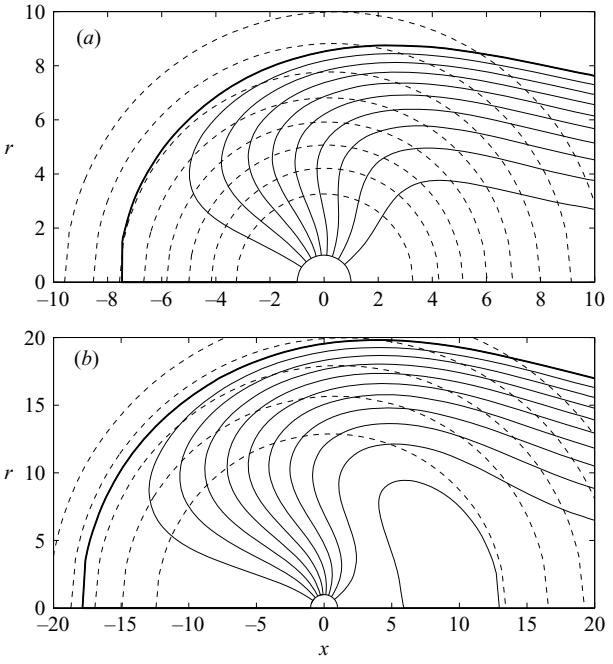

FIGURE 5. The streamlines for the perturbation of the stream function ($\psi'/U = -\lambda$, corresponding to the horizontal axis $\mu = 1, -4\lambda/5, -3\lambda/5, -2\lambda/5, -\lambda/5, 0, 4\lambda/5, 3\lambda/5, 2\lambda/5, \lambda/5$ and λ, the separatrix, the bold curve, corresponding to the stagnating streamline) and the isotherms ((*a*) $\theta = 0$, 0.05, 0.1, 0.15, 0.2, 0.25 and 0.30; (*b*) $\theta = 0$, 0.03, 0.06, 0.09, 0.12 and 0.15), calculated from the large-b_0 (strong-blowing) inner solution for a droplet evaporating steadily in a constant-velocity flow, plotted as solid curves and dashed curves, respectively, for $b_0 = 10$, with (*a*) $\sigma = 1$ and (*b*) $\sigma = 5$.

value which decreases as the vaporization velocity increases. With further increase of b_0, the maximum of vorticity becomes detached from the surface. The curves for $b_0 = 10$ and 50 in figure 7 have approximately the same shape and maximum value, which is located at a radial distance proportional to b_0. This result indicates that, for sufficiently high vaporization velocities, the structure of the velocity field in the mixing region does not change if the problem is appropriately rescaled, as summarized in Appendix B. It may be remarked that, since this large-b_0 behaviour applies only when the mixing layer is in the inner region, the value of ϵ must be small enough that $b_0 \ll 1/\epsilon$, that is, given ϵ the results break down when b_0 becomes too large. Figure 6, for which $b_0 = 1/\epsilon$, violates this inequality for the purpose of illustrating most clearly the characteristics of the streamlines.

5.2. *Force balances and point force*

Once the velocity field in the inner region is obtained, the drag of the droplet can be determined from an integral over the droplet surface. The non-dimensional body force $\boldsymbol{g}$ that appears in (3.2) is of order ϵ^2, so its contribution to the pressure distribution in the inner region can be neglected in the first approximation. Then, the total drag divided by the ratio of the square of the viscosity coefficient to the density can be written as $F = 2\pi \int_{-1}^{1} \{(\boldsymbol{vv} + p\boldsymbol{I} - \boldsymbol{\tau}') \cdot \boldsymbol{e}_r\} \cdot \boldsymbol{e}_x \, \mathrm{d}\mu$, with $\boldsymbol{vv}$ denoting the dyadic product, $\boldsymbol{I}$ the identity matrix and $\boldsymbol{e}_r$ the unity vector in the outward radial direction, where the integrand is evaluated at the droplet surface $r = 1$. This integral can be solved

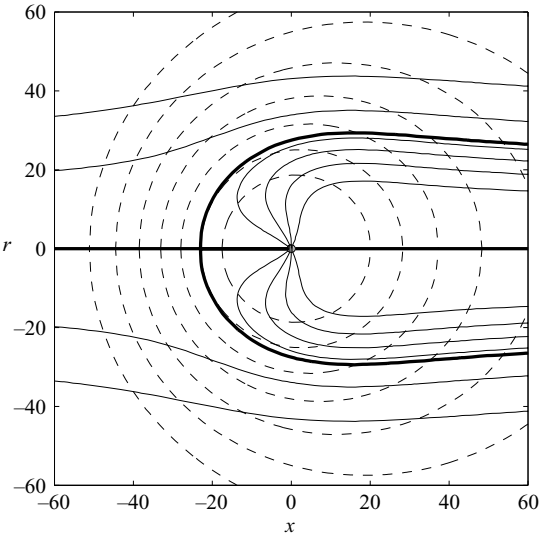

FIGURE 6. The streamlines ($\psi = -b_0 - \epsilon U\lambda$, corresponding to the horizontal line at $r = 0$ for $x > 0$, -5, 0, 5, 10, $b_0 + \epsilon U\lambda$, the separatrix corresponding to the stagnating streamline, 25 and 50), shown as solid curves with the $\mu = 1$ and stagnation streamlines bold, and the isotherms ($\theta = 0$, 0.1, 0.2, 0.3, 0.4, 0.5, 0.6 and 0.7), shown as dashed curves, calculated from the large-b_0 (strong-blowing) inner solution for a droplet evaporating steadily in a constant-velocity flow for $\epsilon U = 0.1$ and $b_0 = 10$, with $\sigma = 5$.

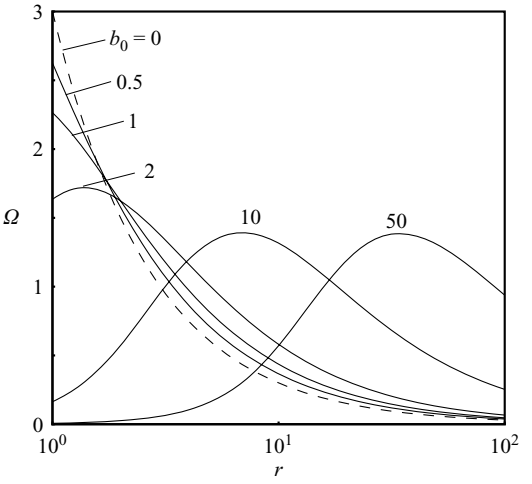

FIGURE 7. The r-dependence of the vorticity factor Ω given by (4.17) for various values of b_0 (solid curves: $b_0 = 0.5$, 1, 2, 10 and 50; dashed curve: $b_0 = 0$) for $\sigma = 1$.

by introducing the expansions for the radial and azimuthal components of the non-dimensional velocity field, $b_0/r^2 + \epsilon U(\lambda/r^2 + \mu f/r^2)$ and $-\epsilon U\sqrt{1-\mu^2}(\mathrm{d}f/\mathrm{d}r)/(2r)$, and the expression of p given by (5.4) for the angular-dependent component in the distribution of the non-dimensional pressure, giving $F = -(2/3)\pi\epsilon U\{f'''(1) + (1 - 2b_0)f''(1) + 4(4 + b_0)f(1)\}$, with f given by (4.11) and the prime denoting differentiation with respect to r. The non-dimensional drag corresponding to the quasi-steady inner

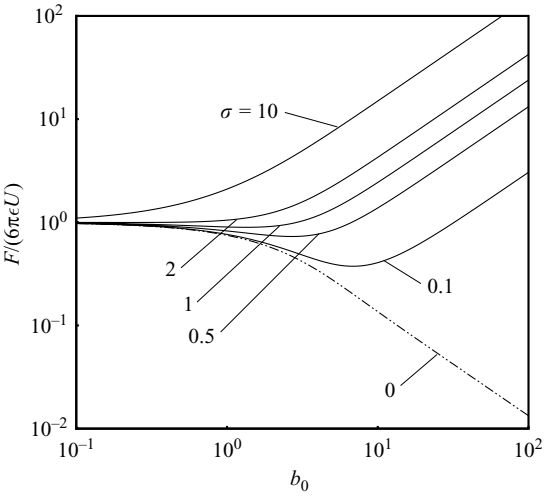

FIGURE 8. Variations with b_0 of normalized drag $F/(6\pi\epsilon U)$, calculated from (5.5), for various values of σ (solid curves: $\sigma = 0.1, 0.5, 1, 2$ and 10; dashed curve: $\sigma = 0$).

velocity field then becomes, up to terms of order ϵ^2,

$$F = 6\pi\epsilon U\left\{\frac{(3+\chi)b_0^3}{9A_1} - \frac{2b_0}{3}\right\} + O(\epsilon^2). \tag{5.5}$$

Figure 8 shows variations of $F/6\pi\epsilon U$, calculated from (5.5), with b_0 for various values of σ. With this normalization, the well-known Stokes drag of a non-vaporizing sphere in steady rectilinear flow corresponds to $F/(6\pi\epsilon U) = 1$, and it is seen in figure 8 that, indeed, $F/(6\pi\epsilon U) = 1$ at $b_0 = 0$ for all values of σ. In this limit, the contribution of the viscous stresses to the drag is dominant and is twice the contribution of the pressure forces, which act in the same direction, that is, the total force arises two-thirds from the viscous stresses and one-third from the pressure.

The curves for $\sigma \leqslant 2$ in figure 8 have negative slope at $b_0 = 0$ and reach a minimum value that decreases with decreasing Prandtl number. However, the curve for $\sigma = 10$ has a positive slope at $b_0 = 0$. Calculating the derivative of F with respect to b_0 at $b_0 = 0$ from (5.5) gives a critical value of $\sigma = 7/3$, above which the drag increases with b_0 monotonically. At lower Prandtl numbers, then, moderate vaporization decreases drag. In the large-b_0 limit, the normalized drag on the droplet is $2b_0\chi_\infty/9$ in the first approximation and is mainly due to the momentum flux ($4b_0\chi_\infty/9$), which is twice the contribution of the pressure forces, which provide thrust (negative drag, $-2b_0\chi_\infty/9$). The viscous stresses have a vanishing net contribution to drag in this limit.

From the quasi-steady momentum conservation equation in the inner region, given by (3.2) with body forces and local time derivatives neglected, it can be shown that $F\boldsymbol{e}_x$ is the total force transmitted to a spherical surface of radius r divided by the product of the density and the square of the kinematic viscosity. The droplet therefore behaves like a point force for large values of r, although this point-force effect is of order ϵ in comparison with the mass-source effect of (5.3). The strength of the point force increases with both b_0 and σ for large b_0, becoming proportional to the vaporization velocity, a measure of the source strength. The initial drag reduction by vaporization at small σ is notable, $F/(6\pi\epsilon U)$ approaching $1 + (3\sigma - 7)b_0$ as b_0 approaches zero. The minimum drag in fact approaches zero as σ approaches zero, and in the limit

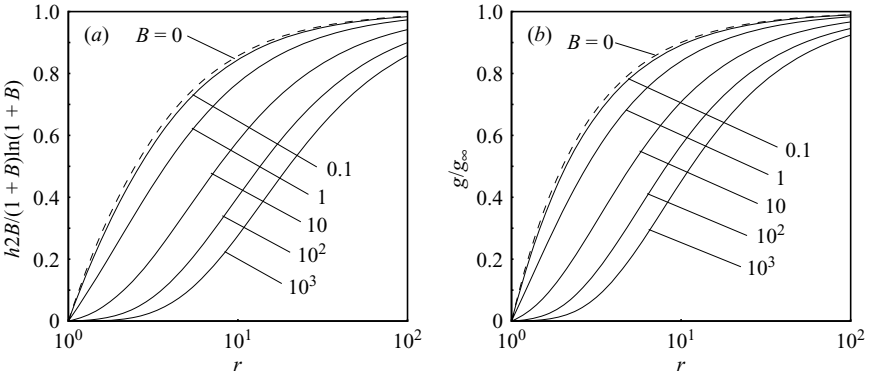

FIGURE 9. Variations with r of (a) the normalized angular-dependent contribution to the temperature field $2Bh/[(1+B)\ln(1+B)]$, calculated from (4.13), and (b) the normalized angular-independent perturbation to the temperature field (g/g_∞), calculated from (4.12), for various values of B (solid curves: $B=0.1$, 1, 10, 10^2 and 10^3; the dashed curves correspond to $h=1/2-3/4r+3/8r^2-1/8r^3$ and $g/g_\infty=1-1/r$, the solution for the non-vaporization limit ($B=0$).

$\sigma=0$ the drag is a monotonically decreasing function of b_0, approaching zero as b_0 approaches infinity. In this limit, the flow near the droplet becomes isothermal and insulated from the external flow. Substantial drag reduction through vaporization therefore can occur at low Prandtl numbers (high thermal conductivities), especially at high vaporization rates.

5.3. *Temperature field and heat sink*

From (4.6), it may be seen that the average perturbation of the inner temperature field is described by the function g, and its angular dependence arises from the function h. It can be shown from (4.13) that as r approaches infinity, h approaches $[(1+B)\ln(1+B)]/(2B)$ for all values of σ. Variations of $2Bh/[(1+B)\ln(1+B)]$ with r for various values of B, calculated from (4.13), are plotted in figure 9(a). The ratio (g/g_∞) is similarly plotted in figure 9(b) as a function of r, with g evaluated from (4.12). The dashed curves in figures 9(a) and 9(b) correspond to $h=1/2-3/4r+3/8r^2-1/8r^3$ and $g/g_\infty=1-1/r$, respectively, which describe the perturbation of the inner temperature in the non-vaporization limit $B=0$, obtained in Appendix B. The gradients of h and g at the surface decrease as B increases. In the strong-vaporization limit, $B\gg1$, variations of the temperature are exponentially small near the surface and begin to be important only at radial distances from the surface of order $\ln(1+B)$.

The asymptotic behaviour of θ for large values of r becomes

$$\theta\sim\theta_\infty-\frac{q_\infty}{r}, \tag{5.6}$$

with

$$\theta_\infty=1+\epsilon U\sigma\left\{g_\infty-\mu\frac{(1+B)\ln(1+B)}{2B}\right\} \tag{5.7}$$

measuring the apparent outer temperature, and

$$q_\infty=\frac{(1+B)\ln(1+B)}{B}+\epsilon U\sigma\left\{g_\infty[1+\ln(1+B)]+\mu\frac{(1+B)\ln(1+B)}{B}B_1\right\} \tag{5.8}$$

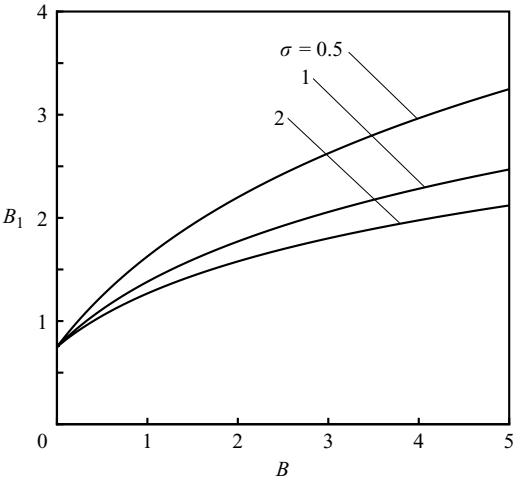

FIGURE 10. Variations of the measure B_1 of the angular dependence of the strength of the heat sink with b_0 evaluated from (5.9) for different values of the Prandtl number ($\sigma = 0.5$, 1 and 2).

the inward heat flux. Equations (5.7) and (5.8) are obtained from (4.1), (4.6) and (4.8)–(4.16) by constructing expansions for large values of r. The constant B_1 in (5.8) can be written as

$$B_1 = \frac{\ln(1+B)}{2} + \frac{(\chi+3)b_0^3}{12A_1}. \tag{5.9}$$

Equations (5.7) and (5.8) exhibit an angular-independent increase of θ_∞ and q_∞ with the transfer number. These increases are proportional to the relative external velocity, to the Prandtl number and to g_∞. The Prandtl-number factor indicates that the Péclet number $\epsilon\sigma$, rather than the Reynolds number ϵ, measures the stregth of these effects. They enhance both the apparent external temperature and the heat flux. Angular-dependent contributions also are present. The apparent temperature is smaller in the downstream direction and larger in the upstream direction, by an amount that increases with increasing B.

The angular variation of q_∞ can be illustrated by plotting B_1 as a function of B, as shown in figure 10 for various values of σ. This figure exhibits a monotonic increase of B_1 with B, indicating an increase of the heat flux with increasing transfer number in the upstream direction and a decrease in the downstream direction with increasing transfer number. Although B_1 decreases with increasing σ in figure 10, the effect of the factor σ in (5.8) is stronger, so that the angular dependence also increases with increasing Prandtl number at fixed Reynolds number. In the non-vaporization limit $B_1 = 3/4$, independent of the Prandtl number.

The non-dimensional total rate of heat transfer $Q = 2\pi \int_{-1}^{1} q_\infty \mathrm{d}\mu$ can be calculated from the solution for q_∞ in (5.8) to be

$$Q = 4\pi\{(1+B)\ln(1+B)/B + \epsilon U\sigma g_\infty[1+\ln(1+B)]\}. \tag{5.10}$$

From (3.3), it can be shown that BQ is the total rate of heat transfer through any spherical surface in the inner zone surronding the droplet divided by the product of the heat of vaporization per unit mass, the viscosity coefficient and the radius of the droplet. Applying this result to large values of r demonstrates that sufficiently far

from its surface the droplet behaves like a point sink of heat, the strength of which increases with increasing B, U, σ and g_∞.

6. The outer solution

In terms of the appropriate rescaled outer variables $R=\epsilon r$, $\boldsymbol{V}=\boldsymbol{v}/\epsilon$, the temperature and streamfunction in the outer region, denoted by $\Theta=\theta$ and $\Psi=\epsilon\psi$, can be written in terms of the expansions

$$\Theta = 1-\epsilon\Theta', \qquad \Psi = \tfrac{1}{2}UR^2(1-\mu^2)+\epsilon\Psi'. \tag{6.1}$$

It is convenient to introduce the outer time variable $\tau=\epsilon^2 t$, the characteristic diffusion time $t_o=ct_e$, according to (2.2), being the appropriate time scale in this region. From (3.3), the non-dimensional temperature perturbation Θ' then satisfies the energy conservation equation

$$\frac{\partial\Theta'}{\partial\tau}+U\frac{\partial\Theta'}{\partial X}-\frac{1}{\sigma}\widetilde{\nabla}^2\Theta' = (Q/\sigma)\delta^3(\boldsymbol{R}), \tag{6.2}$$

with boundary condition $\Theta'\to 0$ at infinity. Here $\widetilde{\nabla}$ denotes the gradient operator defined in (3.10) but based on outer variables, $X=\epsilon x$ denotes the axial coordinate in the outer variables, and δ^3 stands for the delta function in three dimensions. The right-hand side of (6.2) represents a point heat sink located at the centre of the droplet with time-dependent stregth Q given by (5.10).

By changing to a stationary reference system with the origin located at the position of the droplet at $\tau=0$, the solution to (6.2) can be written in terms of the Green's function of the unsteady diffusion equation (Pozrikidis 1997). The solution for Θ' based on coordinates moving with the droplet then becomes

$$\Theta' = \frac{\sqrt{\sigma}}{(4\pi)^{3/2}}\int_{-\infty}^{\tau}\frac{Q(\tau_0)}{\hat{\tau}^{3/2}}\exp\left\{\frac{-\sigma\hat{R}^2}{4\hat{\tau}}\right\}\mathrm{d}\tau_0, \tag{6.3}$$

where $\hat{\tau}=\tau-\tau_0$ is the difference between the actual time and the integration time, $\hat{R}=\{[\mu R-X_d(\tau)+X_d(\tau_0)]^2+(1-\mu^2)R^2\}^{1/2}$ is the distance to the centre of the droplet in stationary coordinates, and $X_d(\tau)=\int_0^\tau U(\tau')\,\mathrm{d}\tau'$ is the axial position of the droplet relative to its position at $\tau=0$.

The asymptotic expansion of Θ' for small values of R must be obtained in order to determine g_∞ by matching with the inner temperature. In accomplishing that, it is not permissible to take the limit $R\to 0$ inside the integral of (6.3) because $\tau_0=0$ is within the limits of integration. Instead, it is necessary to expand asymptotically the integral for small values of R and then take the limit. This can be demonstrated formally by considering the quasi-steady outer temperature generated by a constant-strength heat source Q_0 in a uniform flow at constant velocity U_0. In this case $\hat{R}^2=R^2-2\mu RU_0\hat{\tau}+U_0^2\hat{\tau}^2$, so that the integral in (6.3) can be evaluated exactly to give $\Theta'=[\sigma Q_0/(4\pi)]\exp[-(1-\mu)\sigma R/2]$, which is the quasi-steady outer solution. Taking the limit $R\to 0$ inside the integral of (6.3), however, gives $[\sqrt{\sigma}Q_0/(4\pi)^{3/2}]\times\int_0^\infty\hat{\tau}^{-3/2}\exp(-\sigma\hat{\tau}U_0^2)\,\mathrm{d}\hat{\tau}$ at leading order in R, the integral in which is divergent at its lower limit.

To express results in the most general form, an asymptotic expansion of Θ' for an arbitrary external velocity is helpful. Introducing the expansion for Q given by (5.10) inside the integral in (6.3) leads to an asymptotic expansion of Θ' in terms of ϵ. Expanding the corresponding leading-order term for small values of R, as is explained

with more details in Appendix C, where use is made of the variable $\xi = \sqrt{\sigma/\hat{\tau}}/2$, gives

$$\Theta' \sim \frac{(1+B)\ln(1+B)}{B}\left\{\frac{1}{R} - \Gamma + \mu\frac{\sigma U}{2}\right\} + O(R), \tag{6.4}$$

with

$$\Gamma = \frac{2}{\sqrt{\pi}}\int_0^\infty (1 - \exp(-\sigma Y^2\xi^2))\,\mathrm{d}\xi \tag{6.5}$$

and $Y = \int_{\tau-\sigma/4\xi^2}^{\tau} U(\tau')\,\mathrm{d}\tau'$. The integral in (6.5) must be evaluated numerically for general expressions of the external velocity. The angular-dependent part of the expansion in (6.4) may be seen by comparison with (5.6), (5.7) and (5.8) to match automatically with the inner solution, which is quasi-steady. Only the angular-independent part of the perturbation of the outer temperature depends on the vaporization history through Γ, which is related to g_∞ by matching with the inner solution. Comparing (6.1) and (6.4) with (5.6) and (5.7) demonstrates that matching requires

$$g_\infty U = \frac{b_0(1+B)}{B}\Gamma, \tag{6.6}$$

with b_0 given by (4.2).

In order to obtain closure of the complete solution for the temperature and velocity fields up to terms of order ϵ^2, the first perturbation of the streamfunction Ψ' must also be obtained. To acomplish that, it is convenient to consider the outer velocity field, which can be written in terms of the expansion

$$\boldsymbol{V} = U\boldsymbol{e}_x + \epsilon\boldsymbol{V}'. \tag{6.7}$$

The perturbation $\boldsymbol{V}'$ satisfies the continuity and momentum-conservation equations

$$\widetilde{\nabla}\cdot\boldsymbol{V}' = M\delta^3(\boldsymbol{R}) \tag{6.8}$$

and

$$\frac{\partial\boldsymbol{V}'}{\partial\tau} + \widetilde{U}\frac{\partial\boldsymbol{V}'}{\partial X} + \widetilde{\nabla}P' - \widetilde{\nabla}^2\boldsymbol{V}' = -(F/\epsilon)\boldsymbol{e}_x\delta^3(\boldsymbol{R}), \tag{6.9}$$

with boundary conditions $\boldsymbol{V}' = P' = 0$ at infinity. Here, $P' = p'/\epsilon^2$ denotes the non-dimensional ratio of pressure to density in the outer region. The right-hand sides of (6.8) and (6.9) represent a point mass source and point force, respectively, both located at the centre of the droplet, where the strengths M and F are given by (5.3) and (5.5), respectively.

The solution for $\boldsymbol{V}'$ can be written uniquely by superposition of an irrotational velocity field generated by the mass source and a rotational velocity field generated by the component of the point force associated with the rotational part of the inner velocity field in the absence of the mass source, giving

$$\boldsymbol{V}' = \frac{b_0 + \epsilon g_\infty B/(1+B)}{R^2}\boldsymbol{e}_r + \boldsymbol{V}'_R. \tag{6.10}$$

The first component of $\boldsymbol{V}'$ in (6.10) is purely radial, the associated streamfunction being $-\mu[b_0 + \epsilon g_\infty B/(1+B)]$, which matches with the radial irrotational part of the inner velocity field. Its interaction with the external velocity $U\boldsymbol{e}_x$ has a contribution of $4\pi\epsilon U b_0$ to the strength of the point force F. Therefore, the rotational component of the outer velocity field $\boldsymbol{V}'_R$, which is solenoidal, satisfies the momentum conservation

equation

$$\frac{\partial \boldsymbol{V}'_R}{\partial \tau} + \widetilde{U}\frac{\partial \boldsymbol{V}'_R}{\partial X} + \widetilde{\nabla} P'_R - \widetilde{\nabla}^2 \boldsymbol{V}'_R = 6\pi U \frac{(3+\chi)b_0^3}{9A_1}\boldsymbol{e}_x \delta^3(\boldsymbol{R}), \tag{6.11}$$

with boundary conditions $\boldsymbol{V}'_R = P'_R = 0$ at infinity.

The solution to (6.11) was first obtained by Ockendon (1968) by means of a Fourier transform. He derived an expression for the associated streamfunction, denoted here by Ψ_R, written in terms of a double integral. A simplified expression for Ψ_R was obtained later by Asmolov (2001) in terms of a single integral, in time, of a Green's function. This result can be written, in the notation used here, as

$$\Psi'_R = -\frac{(3+\chi)b_0^4}{12A_1\sqrt{\pi}} \int_{-\infty}^{\tau} \{[2U(\tau_0)\hat{\tau} - \mu R - Y]\exp(-\hat{R}^2/4\hat{\tau}) + \mu R \exp(-R^2/4\hat{\tau})\} \times [\exp(-(1-\mu^2)R^2/4\hat{\tau}) - 1]\frac{\mathrm{d}\tau_0}{\hat{\tau}^{3/2}}, \tag{6.12}$$

where $\hat{\tau}$ and $\hat{R}$ have been defined previously in connection with (6.3). The rescaled vorticity in the outer region, $\widetilde{\omega} = \omega/\epsilon^3$, can be expressed in terms of the outer streamfunction as $\widetilde{\omega} = -\sqrt{1-\mu^2}\widetilde{D}^2\Psi'_R/R$, with $\widetilde{D}^2$ being the operator defined in (3.9) but in terms of outer variables. Introducing the expression for Ψ'_R given by (6.12) into this formula for $\widetilde{\omega}$ gives

$$\widetilde{\omega} = \frac{(3+\chi)b_0^4}{12A_1\sqrt{\pi}}\frac{\sqrt{1-\mu^2}}{R}\int_{-\infty}^{\tau} G(R,\tau,\tau_0)\,\mathrm{d}\tau_0, \tag{6.13}$$

with

$$\begin{aligned} G(R,\tau,\tau_0) = \frac{1}{\hat{\tau}^{3/2}}\Bigg\{ & \left[\frac{2U(\tau_0)\hat{\tau} - Y}{2\hat{\tau}}\left(\frac{\hat{R}^2}{2\hat{\tau}} - 1\right) + \frac{3\mu R - 2Y}{2\hat{\tau}} - \frac{\mu R \hat{R}^2}{4\hat{\tau}^2}\right]\exp(-\hat{R}^2/4\hat{\tau}) \\ & \times (\exp(-(1-\mu^2)R^2/4\hat{\tau}) - 1) + \left[\frac{2U(\tau_0)\hat{\tau} - Y}{2\hat{\tau}}\left(\frac{3R^2}{2\hat{\tau}} - 1\right)\right. \\ & \left. - \frac{\mu^2 R^2[\mu R + Y(1+\mu)]}{4\hat{\tau}^2}\right](1-\mu^2)\exp(-(\hat{R}^2 - (1-\mu^2)R^2)/4\hat{\tau}) \\ & - \left[\frac{3\mu R}{2\hat{\tau}} - \frac{\mu R^3}{4\hat{\tau}^2}\right]\exp(-R^2/4\hat{\tau})(\exp(-(1-\mu^2)R^2/4\hat{\tau}) - 1) \\ & \times \left[\frac{\mu R}{2\hat{\tau}} + \frac{\mu R^3}{2\hat{\tau}^2}\right]\exp(-\mu^2 R^2/4\hat{\tau})\Bigg\}. \end{aligned} \tag{6.14}$$

The asymptotic expansion of Ψ_R for small R can be used to determine perturbations of the velocity field of order ϵ^2 in the inner region. Expanding the integral in (6.12) for small values of R, which is explained with more details in Appendix C, gives

$$\Psi'_R = \frac{(3+\chi)b_0^4}{A_1}\frac{(1-\mu^2)}{12}\left\{U R + \left[\mu\frac{U^2}{4} - \Pi\right]R^2\right\} \tag{6.15}$$

with

$$\Pi = \frac{2}{\sqrt{\pi}}\int_0^{\infty} \xi'^{-2}[(U - 2Y/\xi'^2)\exp(-Y^2\xi'^{-2}) - U(\tau)\exp(\mu R U(\tau)/2)]\,\mathrm{d}\xi'. \tag{6.16}$$

This result can be used to obtain an expansion of Ψ, given by (C18) in Appendix C, which matches with the expansion of ψ for large values of r, given by (C5) in Appendix C.

The expressions obtained for Γ and Π allow for general time variations of the external velocity. Different vaporization histories will result by considering specific problems.

7. Acceleration from rest and deceleration from constant velocity

Specific results for a translating droplet that begins to accelerate from rest or decelerate from constant velocity u_e at $\tau = 0$ are derived in this section. The non-dimensional external velocity can be written in general form as

$$U = U_0 + \gamma c^2 \tau \tag{7.1}$$

for $\tau > 0$ and $U = U_0$ for $\tau < 0$, where U_0 denotes the non-dimensional initial velocity, c denotes the ratio of the characteristic diffusion time in the outer region to the characteristic time of variation of the external velocity, and the two-value parameter γ is 1 for acceleration and -1 for deceleration. If the droplet is initially at rest, U_0 is zero in this notation, and $c = 1$, as explained in deriving (2.3), which applies in this case. If the droplet accelerates or decelerates from constant velocity, U_0 is 1 and $c = \sqrt{d^2 a/(4\nu\epsilon^2 u_e)}$, the initial constant velocity being the velocity scale.

An expression for g_∞ can be obtained from (6.6) by splitting the integral in (6.5) into two parts,

$$\int_0^{\sqrt{\sigma/\tau}/2} + \int_{\sqrt{\sigma/\tau}/2}^{\infty}.$$

The first of these integrals would correspond to $\tau < 0$ in (7.1), so that $U = U_0$ and $Y = U_0\sigma/(4\xi^2)$ according to the definition following (6.5), whereas (7.1) applies for the second integral, and $Y = \sigma[U_0 + \gamma c^2 Y - \sigma/(8\xi^2)]/(4\xi^2)$. The first integral can be expressed in terms of tabulated functions, but the second cannot. In the second, it is useful to define $y = \sqrt{\sigma/\tau}/(4\xi) = \sqrt{\tau/\tau}/2$, and it can then be shown from (6.5) that (6.6) can be written as

$$g_\infty U = \frac{(1+B)\ln(1+B)}{2B}\left\{U_0[1-\mathrm{erf}(U_0\sqrt{\sigma\tau}/2)] + \frac{2}{\sqrt{\sigma\pi\tau}}\left[1+\Lambda-\exp\left(-\sigma U_0^2\tau/4\right)\right]\right\}, \tag{7.2}$$

where

$$\Lambda = \int_0^1 y^{-2}\{1-\exp(-(\sigma/4)\tau y^2[U_0+\gamma c\tau(1-y^2/2)]^2)\}\,\mathrm{d}y. \tag{7.3}$$

For a droplet accelerating from rest $c = 1$ with ϵ given by (2.3), and by putting $z = y\sqrt{\sigma\tau^3}/2$, (7.2) and (7.3) can be simplied to give

$$g_\infty = \frac{(1+B)\ln(1+B)}{2\pi B}\int_0^{\phi(\tau)} z^{-2}\{1-\exp(-z^2[1-z^2/\phi(\tau)^2]^2)\}\,\mathrm{d}z, \tag{7.4}$$

with $\phi(\tau) = \sqrt{\sigma\tau^3}/2$. Numerical integration of this integral produces the solid curves shown in figure 11. According to (5.7), the increase in the apparent external temperature caused by the acceleration is proportional to $\epsilon U\sigma g_\infty$, which, since $U = \tau$ here according to (7.1), is seen from (2.3) and (7.4) to be $(d/2)a^{1/3}(\nu/\sigma)^{-2/3}[(1+B)/B][\ln(1+B)]$ multiplied by a function of $\sigma^{1/3}\tau$, the non-dimensional time variable τ being the physical time multiplied by $(a^2/\nu)^{1/3}$. These results indicate that the relevant parameter for non-dimensionalizing the time is $(a^2\sigma/\nu)^{1/3}$, that is, the thermal diffusivity, rather than the kinematic viscosity, determines the time scale of temperature

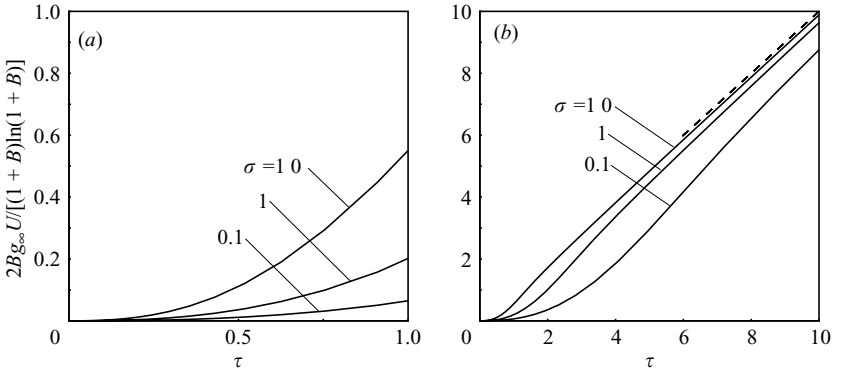

FIGURE 11. Variations of the non-dimensional apparent droplet temperature perturbation $2Bg_\infty U/[b_0(1+B)]$ with the non-dimensional time, the ratio of the time to the characteristic time $(a^2/\nu)^{-1/3}$, evaluated from (7.4) for three different values of the Prandtl number ($\sigma = 0.1$, 1 and 10). $U = \tau$.

evolution under the imposed acceleration. In addition, the Péclet number $(d/2)a^{1/3}(\sigma/\nu)^{2/3}$, rather than the Reynolds number, is the appropriate small parameter, and with these revisions, the dependence on the Prandtl number disappears. The dependence on the transfer number is exactly the same as it is for the quasi-steady problem with a constant imposed external velocity, discussed following (5.7). Until τ becomes of order unity, the droplet is evaporating under the influence of the initial temperature field generated by the evaporating droplet at rest, so that the increase of $g_\infty U$ with time is small, especially at earlier times. The effect of the initial temperature field becomes more important with decreasing Prandtl numbers at fixed kinematic viscosity, since the heat transfer to the inner region increases with the thermal conductivity. For $\tau \gg 1$, the integral in (7.4) approaches $\sqrt{\pi}$, so that the expression for $g_\infty U$ approaches that corresponding to a quasi-steady outer solution, $g_\infty U = [(1+B)\ln(1+B)/2B]\tau$, which is represented by the dashed line in figure 11(*b*).

The case of droplet deceleration from a constant velocity is represented in figure 12, which shows variations of $2Bg_\infty U/[(1+B)\ln(1+B)]$ with time for three different values of σ with $c = 1$. The values of $g_\infty U$ are calculated from (7.2) and (7.3) with $U_0 = 1$ and $\gamma = -1$. At $\tau = 0$, the droplet is evaporating steadily at constant velocity, so the classical result $g_\infty U = \sigma b_0(1+B)/2B$ is obtained. As the external flow decelerates, perturbations of the external temperature tend to move away from the droplet surface so that the rate of heat transfer to the inner region and, therefore, the vaporization rate, decrease. At $\tau = 1$, the droplet is at rest; however, there still is a positive value of $g_\infty U$, which decreases as σ increases for constant kinematic viscosity, indicating that, even in the absence of a convective velocity, there exists a remaining perturbation of the temperature field that increases the vaporization rate in this time-varying situation.

The non-dimensional temperature perturbation in the outer region can be evaluated numerically from (6.3) for these two problems. The results of the numerical integration are shown in figure 13. The temperature decrease with decreasing radius at different times and the approach to the limiting value obtained from (6.6) are readily apparent in this figure, in which the dominant term, proportional to $1/R$ which is seen in (6.4), has been substracted for greater clarity.

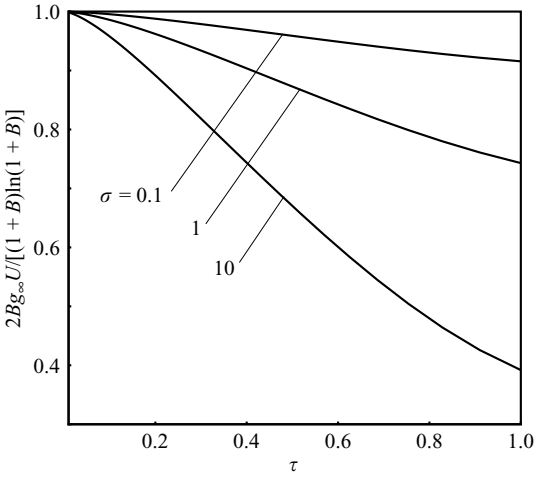

FIGURE 12. Variations of the non-dimensional apparent droplet temperature perturbation $2Bg_\infty U/[b_0(1+B)]$ with non-dimensional time evaluated from (7.2) and (7.3) for three different values of the Prandtl number ($\sigma = 0.1$, 1 and 10) and $c = 1$, $U_0 = 1$ and $\gamma = -1$. $U = 1 - \tau$.

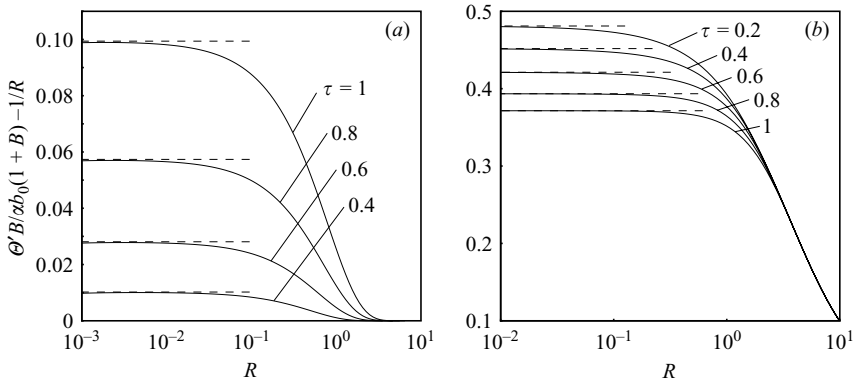

FIGURE 13. Variations of the non-dimensional apparent droplet temperature perturbation $\Theta' B/(\sigma b_0(1+B)) - 1/R$ with the non-dimensional radius R, obtained by numerical evaluation of (6.3) and values of $g_\infty U B/[b_0(1+B)]$, calculated from (6.6), for (*a*) droplet acceleration from rest ($U_0 = 0$, $\gamma = 1$), and for (*b*) droplet deceleration from constant velocity ($U_0 = 1$, $\gamma = -1$). (*a*) $U = \tau$, $\sigma = 1$, $\mu = 0$. (*b*) $U = 1 - \tau$, $\sigma = 1$, $\mu = 0$.

8. Oscillatory motion

For a droplet evaporating in oscillatory motion, the non-dimensional external velocity can be written in general form as

$$U = U_m + W\cos(c\tau), \tag{8.1}$$

with U_m denoting the mean velocity, W the constant amplitude and c the non-dimensional frequency normalized with the inverse of the characteristic diffusion time in the outer region t_o^{-1}. Typically, the mean velocity is used as the velocity scale, so that $U_m = 1$ in this notation. For pure oscillatory motion with zero mean velocity ($U_m = 0$), the amplitude of the velocity fluctuations becomes the appropriate velocity scale; therefore $W = 1$. Introducing the definition of U in (8.1) into (6.5) gives an

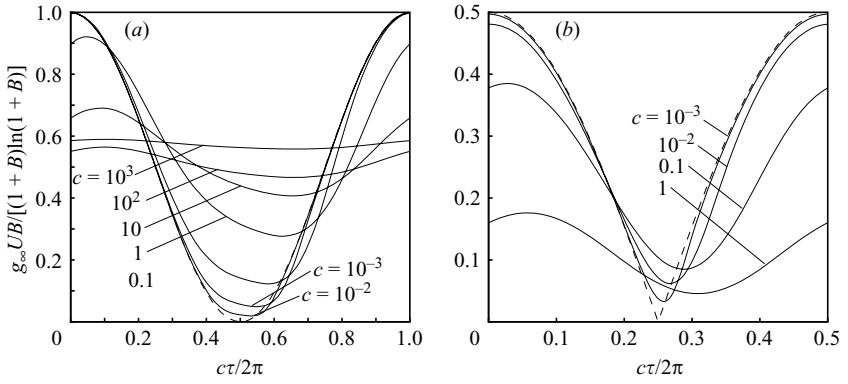

FIGURE 14. Variations of the non-dimensional apparent droplet temperature perturbation $Bg_\infty U/[b_0(1+B)]$ with the non-dimensional time τ for oscillatory external velocity calculated from (8.2) over one period of oscillation, for $\sigma = 1$ and different values of the non-dimensional frequency c for (a) oscillatory motion with mean velocity and $W = 1$ for $c = 10^{-3}$, 10^{-2}, 10^{-1}, 1, 10, 10^2 and 10^3 ($u = 1 + \cos(c\tau)$), and for (b) pure oscillatory motion with zero mean velocity and $c = 10^{-3}$, 10^{-2}, 10^{-1} and 1 ($U = \cos(c\tau)$).

expression for $g_\infty U$ that can be written as

$$g_\infty U = \frac{(1+B)\ln(1+B)}{B} \times \frac{2}{\sqrt{\pi}} \int_0^\infty \left[1 - \exp\left\{-\left(\frac{U_m y}{4} + \frac{\sigma W}{cy}[\sin(c\tau) - \sin(ct - cy^2/4)]\right)^2\right\}\right] \frac{\mathrm{d}y}{y^2}, \quad (8.2)$$

where the integral must be evaluated numerically. Variations of $Bg_\infty U/[\sigma(1+B)]$ for oscillatory external velocity calculated from (8.2) are plotted as functions of a normalized time in figure 14 over one period of oscillation, for $\sigma = 1$ and different values of c. Figure 14(a) represents the case of oscillatory motion with non-zero mean velocity for the case $W = 1$, and figure 14(b) represents the case of pure oscillatory motion with zero mean velocity. In the limit $c = 0$, it can be shown from (8.2) that $g_\infty U = [(1+B)\ln(1+B)/(2B)]|U_0 + W\cos(c\tau)|$, which is the result corresponding to a quasi-steady outer solution, plotted as dashed curves in figure 14 for the two cases represented there. For any other frequency of the external velocity represented in figure 14, $g_\infty U$ is periodic with frequency c, the amplitude decreasing and the phase shifting so that the maximum of the apparent temperature occurs at later times as the frequency increases. The results in figure 14(a) are different from the results obtained by Pozrikidis (1997) for pure uniform oscillatory motion, in which there is no phase shift as the frequency increases. Except for this difference, the discussion by Pozrikidis (1997) applies.

9. Conclusions

The first-order asymptotic analysis presented here shows that the solution near the surface of a droplet evaporating in a slowly varying flow at low Reynolds number is quasi-steady except during short periods of time, of the order of the characteristic diffusion time based on the droplet diameter, when the droplet acceleration changes abruptly. The unsteadiness caused by the time variation of the relative velocity between the droplet and the external flow affects only the perturbation of the temperature and velocity field in the Oseen region, written in terms of time-history integrals, and the

vaporization rate through the angular-independent apparent external temperature, which increases with increasing external velocities.

Explicit closed-form expressions for the quasi-steady perturbations of the temperature and the velocity field in the inner region have been written in terms of the transfer number, the Prandtl number and the non-dimensional time, in simpler forms than those that can be found in the literature, revealing various properties of the solution in this region not seen before. With the non-dimensionalization adopted, the unperturbed non-dimensional vaporization rate b_0 decreases with increasing Prandtl number as a consequence of the dimensional vaporization rate being independent of viscosity. Lower thermal conductivities and larger transfer numbers increase the perturbation of the vaporization rate, by increasing the apparent external temperature, and enhance its angular dependence, the vaporization rate becoming larger in the upstream direction and smaller in the downstream direction. For Prandtl numbers below the critical value $\sigma = 7/3$, the drag decreases with b_0 for low and moderate vaporization rates, reaching a minimum that decreases with decreasing Prandtl number. In the limit $\sigma = 0$, the drag is a monotonically decreasing function of b_0 and vanishes as b_0 tends to infinity. For large vaporization velocities, the vorticity region is blown away from the droplet surface, the solution in the vicinity of the droplet becoming isothermal and irrotational. In this large-b_0 limit, a transition mixing region develops at radial distance of order b_0^{-1} as a result of the interaction of the source flow with the externally imposed uniform flow, creating a negative pressure gradient in the tangential direction on the droplet side that reverses the flow. The velocity and pressure fields near the droplet surface in the strong-vaporization limit depend only on the Prandtl number through the angular-dependent part of the vaporization rate, as does the drag, which decreases with the Prandtl number and is mainly due to momentum, pressure forces having a negative contribution to the drag.

Sufficiently far from its surface, the droplet behaves like a point source of mass and heat, their strength increasing with the external velocity, the transfer number and the thermal conductivity, and like a point force pointing upstream in the axial direction and with strength equal to the drag. These results allow the solutions in the Oseen region to be written as single time-history integrals of Green's functions. Particular results for a translating droplet that accelerates slowly from rest reveal that, until times of the order of the characteristic diffusion time in the Oseen region, the droplet evaporates under the influence of the initial temperature field generated by the droplet evaporating at rest and the apparent external temperature is smaller than that corresponding to a quasi-steady solution, higher thermal conductivities increasing this effect. If the droplet decelerates from constant velocity, the heat transfer and, consequently, the vaporization rate decrease more slowly than those corresponding to a quasi-steady solution. Perturbations of the temperature in the Oseen region remain even in the absence of forced convection, higher thermal conductivities increasing the apparent external temperature. For a droplet moving in oscillatory motion, it is seen that the time variation of the apparent external temperature is periodic with the same frequency as that of the external velocity, but the amplitude decreases and the phase lags as the frequency increases.

These results provide a first step towards addressing theoretically the vaporization and combustion of fuel droplets in slowly varying flow at low Reynolds numbers. In droplet combustion, the effect of heat release associated with the chemical reactions creates typically large variations of temperature within the flow field, so that the dependence of the density and the transport properties on the temperature must be included in the analysis. Different limits appear in this problem depending on

the location of the flame relative to the droplet surface, which is determined by a parameter S, the stoichiometric mass of oxidizer consumed per unit mass of fuel. For large S, the flame is in the Oseen region, whereas for S of order unity or smaller, it is in the Stokes region. Hermanns (2006) addresses the limiting case of large S, typical in the combustion of liquid hydrocarbon fuels in air, and Péclet numbers of order S^{-1}. In this work, the solutions are written in terms of matched asymptotic expansions, using the Péclet number as the small parameter. Since the thermal expansion occurring in the outer region produces large variations of density, the analysis of the Oseen region must be carried out numerically, but the matching can be done analytically to provide the boundary conditions required for the numerical integrations. For values of S of order unity, the outer region is simpler, but there are correspodingly large variations of density in the vicinity of the droplet surface that requires significant computational work. Numerical analysis of distinguished regions with analytical matching thus seem to constitute a fruitful future path for analysis of droplet combustion.

We are greatly indebted to Amable Liñàn and Miguel Hermanns for helpful discussions in the course of this work. Related discussions with Vedha Nayagam, Constantine Pozrikidis, and Stefan Llewellyn Smith are also greatly appreciated. This research was supported by the NASA Microgravity Combustion Science program.

Appendix A. The constants of integration of the quasi-steady inner solution

The constant of integration K_1, K_2, K_3 and K_4 in (4.8) and (4.16) can be written as

$$K_1 = \frac{2}{(\sigma b_0)^2}(\sigma b_0 - 1 + \mathrm{e}^{-b_0\sigma}), \tag{A 1}$$

$$K_2 = \frac{2}{(\sigma b_0)^3}[\sigma b_0 - 2 + (\sigma b_0 + 2)\,\mathrm{e}^{-\sigma b_0}], \tag{A 2}$$

$$K_3 = \frac{2}{(\sigma b_0)^3}\left[\tfrac{1}{2}(\sigma b_0)^2 - 2\sigma b_0 + 3 - (\sigma b_0 + 3)\,\mathrm{e}^{-\sigma b_0}\right] \tag{A 3}$$

and

$$\begin{aligned} K_4 = \frac{1}{30\sigma^3 b_0^2}\big\{ & [\sigma^5 \ln(\sigma^{-1}+1) + (10\sigma^2 + 15\sigma + 6)\ln(1+\sigma) - \sigma^4 + \sigma^3/2 - 12\sigma^2 - 6\sigma]b_0^4 \\ & - 10\sigma^2 b_0^3 + 10\sigma b_0^2 + 4\sigma^2 b_0 - 6\sigma + \left[-\sigma^2 b_0^5 + (\sigma^2 + 4\sigma)b_0^4 + (8\sigma^2 + 11\sigma)b_0^3\right. \\ & \left. - (4\sigma^2 + 7\sigma)b_0^2 - (4\sigma^2 - 6\sigma)b_0 + 6\sigma\right]\mathrm{e}^{-b_0} + \left[\sigma^4 b_0^3 - (\sigma^3 + 10\sigma)b_0^2 + 2\sigma^2 b_0 + 6\sigma\right] \\ & \times \mathrm{e}^{-\sigma b_0} + \left[2\sigma b_0^4 - (\sigma^4 - \sigma^3 + \sigma^2 + 11\sigma)b_0^3 + (\sigma^3 - 2\sigma^2 + 7\sigma)b_0^2 - 2(\sigma^2 + 3\sigma)b_0\right. \\ & \left. - 6\sigma\right]\mathrm{e}^{-(1+\sigma)b_0} + \left[\sigma^2 b_0^2 - 4\sigma b_0 - 10\sigma^2 - 15\sigma - 2(\sigma b_0 + 3)\mathrm{e}^{-\sigma b_0} - b_0 K_3/30\right]b_0^4 E_1(b_0) \\ & - \sigma^5 b_0^4 E_1(\sigma b_0) + (\sigma^5 + 10\sigma^2 + 15\sigma + 6)b_0^4 E_1[(1+\sigma)b_0]\big\}, \end{aligned} \tag{A 4}$$

with

$$E_1(x) = \int_x^\infty \frac{\mathrm{e}^{-t}}{t}\,\mathrm{d}t, \tag{A 5}$$

which is related to the exponential integral (Abramovitz & Stegun 1965). The first three of these, which are plotted in figure 15, depend only on the product σb_0, that is, they are determined uniquely by the single parameter B. The fourth, which depends on both B and σ, is plotted in figure 16 for different values of σ. As B approaches infinity, the values of K_1, K_2 and K_3 all approach zero, while K_4 diverges

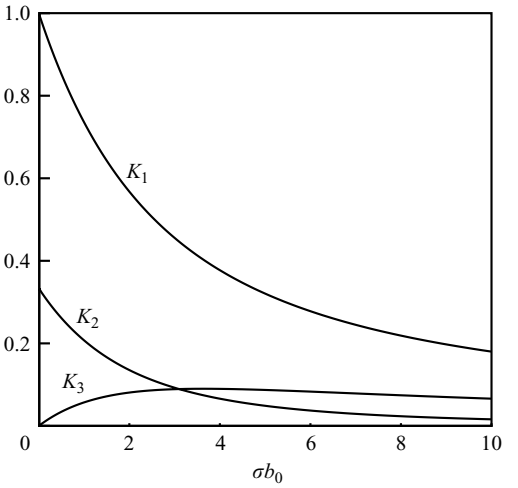

FIGURE 15. Variations of the integration constants K_1, K_2 and K_3, given by (A1), (A2) and (A3), with the product σb_0 related to the transfer number.

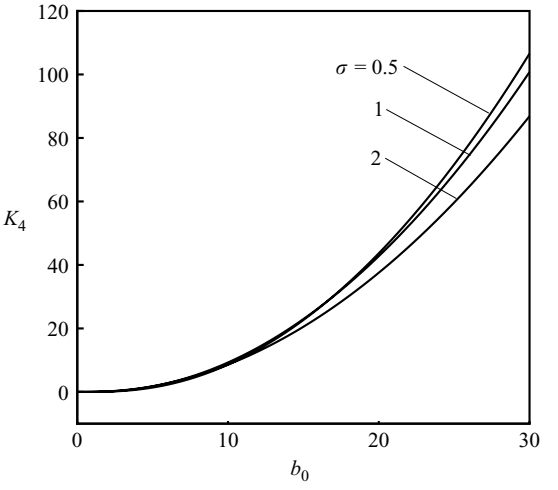

FIGURE 16. Variations of the integration constant K_4, given by (A4), with the unperturbed non-dimensional vaporization rate b_0 for various values of the Prandtl number ($\sigma = 0.5$, 1 and 2).

(in proportion to B^2). At $B = 0$, K_3 and K_4 vanish, but K_1 and K_2 are positive. Typically, K_1 is the largest and most important of these four functions, while K_2 is the second most important, although all four have significant effects on the solution.

Appendix B. The limits of weak and strong vaporization

The limiting case of weak vaporization of the droplet, $b_0 \ll 1$, is a regular perturbation problem at the leading orders. The solutions in the inner region can be written as series of powers of b_0 by expanding the expressions for λ, χ, f, g and h in (4.7), (4.8) and (4.11)–(4.13) for small b_0. The constants A_1 and A_2 in (4.9) and (4.10) and the constants K_1, K_2, K_3 and K_4 in (A1)–(A4) can be expanded for small b_0, giving

$A_1 = b_0^3/3 - b_0^4/8 + O(b_0^5)$, $A_2 = b_0^3/6 - b_0^4/8 + O(b_0^5)$, $K_1 = 1 - \sigma b_0/3 + \sigma^2 b_0^2/12 + O(b_0^3)$, $K_2 = 1/3 - \sigma b_0/6 + O(b_0^2)$, $K_3 = \sigma b_0/12 - \sigma^2 b_0^2/30 + O(b_0^3)$ and $K_4 = \sigma b_0^4/36 - (2\sigma^2 + 3\sigma) b_0^5/216 + O(b_0^5 \ln b_0)$. Introducing these results into (4.8) and expanding for small b_0 gives

$$\chi = \frac{3\sigma b_0}{8} + O(b_0^2). \tag{B 1}$$

The integral in (4.11) can be expanded for small b_0 and values of r of order unity giving $(r^5-1)/(5b_0^5) - (r^3-1)/(6b_0^3) + (r^2-1)/(6b_0^2) - (r-1)/(8b_0) + O(\ln r)$. Employing this result and the expansions of χ and A_1 in (4.11) gives, at leading order in b_0,

$$f = r^2 + \frac{1}{2r} - \frac{3r}{2} + \frac{3}{16}\left[6 - (3+\sigma)\left(\frac{1}{r} + r\right)\right] b_0 + O(b_0^2). \tag{B 2}$$

The corresponding expansion for g in Eq. (4.12) is

$$g = g_\infty (1 - 1/r)(1 - \sigma b_0/r) + O(b_0^2), \tag{B 3}$$

and from (4.13) and (B2),

$$h = \frac{1}{2} - \frac{3}{4r} + \frac{3}{8r^2} - \frac{1}{8r^3} + O(b_0). \tag{B 4}$$

Through (4.6) and other equations, these results determine the velocity and temperature fields for non-vaporizing and weakly vaporizing droplets. In particular, the first term in (B2) gives the well-known Stokes streamfunction for flow around a solid sphere, and the second term is the correction for weak vaporization.

The limiting case of strong vaporization, $b_0 \gg 1$, is somewhat more involved. Near the droplet surface, the solutions for g and h are exponentially small, implying temperatures determined by the unperturbed spherically symmetrical temperature field, and f can be expanded in powers of b_0^{-1} to obtain

$$f = -\frac{\chi_\infty}{3}\left(r^2 + \frac{2}{r}\right) + O(b_0^{-1}), \tag{B 5}$$

with χ_∞ given by (5.2). Then, at leading order in b_0^{-1}, the solution near the surface becomes isothermal and irrotational, the flow being purely radial in the first approximation.

At radial distance of order b_0, for large b_0, the solution can be written in the appropriate rescaled variables $\bar{r} = r/b_0$, $\bar{f} = f/b_0^2$, $\bar{g} = g/b_0$ and $\bar{h} = h/b_0$. Then, at leading order in b_0^{-1}, the inner solution in this region can be written as

$$\bar{f} = 2(3 + \chi_\infty)\left[\frac{\bar{r}^4}{5} - \frac{1}{\bar{r}}\int_0^{\bar{r}} (\xi^3 + \xi^4)\, \mathrm{e}^{-1/\xi}\, \mathrm{d}\xi\right] - \chi_\infty \frac{\bar{r}^2}{3}, \tag{B 6}$$

$$\bar{g} = \bar{g}_\infty e^{-\sigma/\bar{r}}, \tag{B 7}$$

with $\bar{g}_\infty = g_\infty/b_0$, and

$$\bar{h} = \left[\int_0^{\bar{r}} \left(\frac{2\xi}{\sigma} - 1\right)\frac{\bar{f}\, \mathrm{d}\xi}{\xi^2}\right]\left(\frac{2\bar{r}}{\sigma} + 1\right)\mathrm{e}^{-\sigma/\bar{r}} - \left[\int_0^{\bar{r}} \left(\frac{2\xi}{\sigma} + 1\right)\frac{\bar{f}\, \mathrm{e}^{-\sigma/\xi}\, \mathrm{d}\xi}{\xi^2}\right]\left(\frac{2\bar{r}}{\sigma} - 1\right). \tag{B 8}$$

The vorticity function written in (4.17) can be seen to depend directly only on $\bar{r}$, apart from a scaling prefactor, just σ-dependent, determining its strength. These solutions describe the flow and temperature fields associated with the interaction of a point source with a uniform flow at a temperature different from that of the source.

Appendix C. Calculations required for obtaining the composite solutions for the streamfunction and temperature

In order to match the inner and outer solution, the asymptotic expansions of θ and ψ for large r and of Θ and Ψ for small R must be obtained. To derive the θ expansion for large r, the expressions for θ_0, g and h from (4.2), (4.12) and (4.13) can be expanded in the large-r limit to give, up to terms of order $1/r^2$

$$\theta_0 = 1 - \frac{(1+B)\ln(1+B)}{B}\frac{1}{r}, \tag{C 1}$$

$$g = g_\infty\{1 - [1+\ln(1+B)](1/r)\}, \tag{C 2}$$

$$h = \frac{(1+B)\ln(1+B)}{B}\left\{\frac{1}{2} + \frac{B_1}{r}\right\}, \tag{C 3}$$

with B_1 given by (5.9). Combinig these results according to (4.1) and (4.6), the asymptotic expansion of θ for large r can be expressed as

$$\theta \sim \theta_\infty - \frac{q_\infty}{r}, \tag{C 4}$$

with θ_∞ and q_∞ given by (5.7) and (5.8) in the main text. To obtain the ψ expansion for large r, the asymptotic expansion of the integral in (4.11) for large r can be written as $(r^5-1)/(5b_0^5) - (r^3-1)/(6b_0^3) + (r^2-1)/(6b_0^2) - (r-1)/(8b_0) + O(\ln r)$, leading to an expansion of f which can be used with (4.1), (4.2) and (4.5) to show that

$$\psi = -\mu b_0 + \epsilon U\left\{-\frac{\mu g_\infty B}{1+B} + \frac{1-\mu^2}{2}\left[r^2 + \frac{b_0^3(3+\chi)}{6A_1}\left(r + \frac{3b_0}{4}\right) + \left(\frac{(3+\chi)b_0^4}{8A_1} - (1+\chi)\right)\frac{1}{r}\right]\right\}. \tag{C 5}$$

By introducing the expansion for Q given by (5.10) inside the integral in (6.3) and changing to a more convenient variable $\zeta = R/\sqrt{4\hat{\tau}/\sigma}$, at leading order in ϵ the expression

$$\Theta' = \frac{\sigma b_0(1+B)}{BR}\sqrt{\frac{4}{\pi}}\int_0^\infty \exp[-\zeta^2(1 - 2\mu Y R^{-1} + Y^2R^{-2})]\,\mathrm{d}\zeta \tag{C 6}$$

is obtained, with $Y = X_d(\tau) - X_d(\tau - \sigma R^2/4\zeta^2)$. An asymptotic expansion of the integral in (C6) for small values of R can be obtained by breaking the integral into two parts, $\int_0^\lambda + \int_\lambda^\infty$, with $R \ll \lambda \ll 1$. Since $U = \mathrm{d}X_d/\mathrm{d}\tau$, use of a Taylor expansion in the expression for Y shows that the approximation $Y = \sigma U R^2/(4\zeta^2)$ is valid in the interval $\lambda < \zeta < \infty$, reducing the argument of the exponential in (C6) to $-\zeta^2 + \mu\sigma U R/2 - \sigma^2U^2R^2/(16\zeta^2)$, so that the second of these integrals becomes proportional to $\mathrm{erfc}(\lambda)$ and, in the limit of small λ, approaches $(\sqrt{\pi}/2)(1+\mu\sigma U R/2)$ when expanded to first order for small R. In the first integral, an appropriate variable is $\xi = \zeta/R$, in terms of which this integral becomes, up to terms of order R^2, $R\int_0^{\lambda/R}\exp[-Y\xi^2(Y - 2\mu R)]\,\mathrm{d}\xi$, in which $Y = \int_{\tau-\sigma/4\xi^2}^{\tau} U(\tau')\,\mathrm{d}\tau'$ in the present variables. Since Y is seen from this expression to become proportional to ξ^{-2} for large ξ, the leading-order term in the argument of the exponential for small R vanishes for large ξ, causing the exponential to approach unity and the integral to diverge as λ/R approaches infinity. It is therefore appropriate to add and subtract $R\int_0^{\lambda/R}\mathrm{d}\xi = \lambda$, obtaining, up to terms of order R^2, $\lambda - R\int_0^{\lambda/R}(1 - \exp(-Y^2\xi^2))\,\mathrm{d}\xi$, which, in the limit of vanishing λ and R/λ, approaches $\sqrt{\pi}R\Gamma/2$, with Γ defined by (6.5), a convergent integral. Combining these results

produces an asymptotic expansion of Θ' for small values of R, given by (6.4), which can be introduced into (6.1) to give, up to terms of order ϵ^2, the expansion

$$\Theta = 1 - \epsilon \frac{\sigma b_0(1+B)}{B}\left\{\frac{1}{R} - \Gamma + \mu\frac{\sigma U}{2}\right\} + O(R). \tag{C 7}$$

The procedure used to obtain the expansion in (C7) can be followed to expand the integral in (6.12), as well, which can be written in terms of $\zeta' = R/\sqrt{4\hat{\tau}}$ and Y to give

$$\Psi_R' = -\frac{(3+\chi)b_0^4}{3A_1\sqrt{\pi}}\int_0^\infty H(\tau, \zeta')\,\mathrm{d}\zeta', \tag{C 8}$$

with

$$H(\tau,\zeta') = [(UR/2\zeta'^2 - \mu - Y/R)\exp(-\zeta'^2(1 - 2\mu Y R^{-1} + Y^2R^{-2})) + \mu\exp(-\zeta'^2] \times [\exp(-(1-\mu^2)\zeta'^2) - 1]. \tag{C 9}$$

An asymptotic expansion of Ψ_R' for small values of R can be obtained by breaking the integral in (C9) into two parts, $\int_0^\lambda + \int_\lambda^\infty$. Introducing the approximation $Y = UR^2/(4\zeta'^2)$ in the second of these integrals gives $-[I_1(a,\lambda) - I_1(\mu a, \mu\lambda)] + [\mu I_2(a,\lambda) - I_2(\mu a, \mu\lambda)$, with $a = UR/4$,

$$I_1(a,\lambda) = \frac{\sqrt{\pi}}{4}\left\{\mathrm{e}^{2(1+\mu)a}[1 + \mathrm{erf}(\lambda + a/\lambda)] - \mathrm{e}^{-2(1-\mu)a}[1 + \mathrm{erf}(\lambda - a/\lambda)]\right\}, \tag{C 10}$$

and

$$I_2(a,\lambda) = \frac{\sqrt{\pi}}{4}\left\{\mathrm{e}^{-2(1-\mu)a}[1 - \mathrm{erf}(\lambda - a/\lambda)] + \mathrm{e}^{2(1+\mu)a}[1 - \mathrm{erf}(\lambda + a/\lambda)] - 2[1 + \mathrm{erf}(\lambda)]\right\}. \tag{C 11}$$

The expressions for $I_1(\mu a, \mu\lambda) - I_1(a,\lambda)$ and $\mu I_2(a,\lambda) - I_2(\mu a, \mu\lambda)$ can be expanded for small a, λ and a/λ. Neglecting higher-order terms gives

$$I_1(\mu a, \mu\lambda) - I_1(a,\lambda) = \sqrt{\pi}a(\mu - 1) - \lambda a\,\mathrm{e}^{2\mu a}(1-\mu^2) + \sqrt{\pi}2a^2\mu(\mu - 1) - \frac{a^3}{\lambda}\mathrm{e}^{2\mu a}(1-\mu^2) \tag{C 12}$$

and

$$\mu I_2(a,\lambda) - I_2(\mu a, \mu\lambda) = \frac{\sqrt{\pi}}{2}(\mu - 1)(\mathrm{e}^{2\mu a} - 1) + \sqrt{\pi}a^2\mu(1-\mu) + \tfrac{2}{3}a\lambda^3\mu^2(1-\mu^2) - \frac{a^4}{2\lambda}\mu(1-\mu^2). \tag{C 13}$$

The first integral becomes $R^3(1-\mu^2)[J_1 + \mu R J_2]$, with

$$J_1 = \int_{R/\lambda}^\infty \xi'^{-4}[2U(\tau - \xi'^2/4)\xi'^2/4 - Y]\exp\{-Y\xi'^{-2}[Y - 2\mu R]\}\,\mathrm{d}\xi', \tag{C 14}$$

$$J_2 = \int_{R/\lambda}^\infty \xi'^{-4}[1 - \exp\{-Y\xi'^{-2}[Y - 2\mu R]\}\,\mathrm{d}\xi', \tag{C 15}$$

where $\xi' = R/\zeta'$. The integrals J_1 and J_2 are divergent in the limit of vanishing R/λ. If $(a/R)\,\mathrm{e}^{\mu 2a}\int_{R/\lambda}^{\infty}\xi'^{-2}\,\mathrm{d}\xi'$ is added to and subtracted from J_1, it is found that

$$J_1 = \int_{R/\lambda}^{\infty}\{\xi'^{-4}[2U(\tau-\xi'^2/4)\xi'^2/4 - Y]\exp(-Y\xi'^{-2}[Y-2\mu R]) - (a/R)\exp(\mu 2a)\xi'^{-2}\}\,\mathrm{d}\xi' + a\lambda\exp(2\mu a)/R^2. \quad (C\,16)$$

The last integral is convergent in the limit $R/\lambda \to 0$, so it can be split as $\int_0^{\infty} - \int_0^{R/\lambda}$. Using the approximation $Y = U\xi'^2/4$ in the second of the last integrals gives $a^3R^{-2}\exp(2\mu a)/\lambda + O(R^2)$. Adding and subtracting $\int_{R/\lambda}^{\infty}\{[1-\exp(2\mu a)]\xi'^{-4} + a^2\xi'^{-2}]\,\mathrm{d}\xi'$ from J_2 gives

$$J_2 = \int_{R/\lambda}^{\infty}\{\xi'^{-4}[\exp(2\mu a) - \exp\{-Y\xi'^{-2}[Y-2\mu R]\}] - a^2\xi'^{-2}/R^2\}\,\mathrm{d}\xi' + (1-\exp(2\mu a))\lambda^3/3R^3 + a^2\lambda/R^3. \quad (C\,17)$$

The last integral is convergent, so it can be split as $\int_0^{\infty} - \int_0^{R/\lambda}$. The second of these integrals can be expanded to give $-a^4/(2R^3\lambda)$. Combining these results gives an asymptotic expansion of Ψ_R' for small values of R, given by (6.15), which can be introduced into (6.1) to give, up to terms of order ϵ^2, the expansion

$$\Psi = \frac{1}{2}UR^2(1-\mu^2) + \epsilon\left\{-\mu b_0 + \frac{(\chi+3)b_0^4}{A_1}\frac{(1-\mu^2)}{12}\left[UR + \mu\frac{U^2}{4} - \Pi\right]R^2\right\}, \quad (C\,18)$$

where

$$\Pi = \frac{2}{\sqrt{\pi}}\int_0^{\infty}\xi'^{-2}[(U - 2Y/\xi'^2)\exp(-Y^2\xi'^{-2}) - U(\tau)\exp(\mu RU(\tau)/2)]\,\mathrm{d}\xi' \quad (C\,19)$$

and the term $-\mu b_0$ inside the square brackets in (C18) corresponds to the leading-order term in ϵ of the streamfunction associated with the first component of $\boldsymbol{V}'$ in (6.10).

REFERENCES

Abramovitz, M. & Stegun, I. A. 1965 *Handbook of Mathematical Functions*, p. 228.

Abramzon, B. & Elata, C. 1984 Unsteady heat transfer from a single sphere in Stokes flow. *Intl J. Heat Mass Transfer* **27**, 687–695.

Ackerman, M. D. & Williams. F. A. 2005 A simplified model for droplet combustion in a slow convective flow. *Combust. Flame* **143**, 599–612.

Acrivos, A. & Taylor, T. D. 1962 Heat and mass transfer from single spheres in Stokes flow. *Phys. Fluids* **5**, 387–394.

Asmolov, E. S. 2001 Flow past a sphere undergoing unsteady rectilinear motion and unsteady drag at small Reynolds number. *J. Fluid Mech.* **446**, 95–119.

Batchelor, G. K. 1979 Mass transfer from a particle suspended in fluid with a steady linear ambient velocity distribution. *J. Fluid Mech.* **95**, 369–400.

Brenner, H. 1963 Forced convection heat and mass transfer at small Peclet numbers from a particle of arbitrary shape. *Chem. Engng Sci.* **18**, 63–148.

Chiu, H. H. 2000 Advances and challenges in droplet and spray combustion. I. Towards a unified theory of droplet aerothermochemistry. *Prog. Energy Combust. Sci.* **26**, 381–416.

Choudhury, P. N. & Drake, D. G. 1971 Unsteady heat transfer from a sphere in a low Reynolds number flow. *Q. J. Mech. Appl. Maths* **24**, 23–36.

Chung, J. N., Ayyaswamy, P. S. & Sadhal S. S. 1984 Laminar condensation on a moving drop. Part 1. Singular perturbation technique. *J. Fluid Mech.* **139**, 105–130.

Clift, R., Grace, J. R. & Weber, M. E. 1978 *Bubbles, Drops, and Particles*. Academic.

Crespo, A. & Liñán, A. 1975 Unsteady effects in droplet evaporation and combustion. *Combust. Sci. Technol.* **11**, 9–18.

Dwyer, H. A. 1989 Calculation of droplet dynamics in high temperature environment. *Prog. Energy Combust. Sci.* **15**, 131–158.

Faeth, G. M. 1977 Current status of droplet and liquid combustion. *Prog. Energy Combust. Sci.* **3**, 191–234.

Fendell, F. E. 1968 Decompositional burning of a droplet in a small Peclet number flow. *AIAA J.* **6**, 1946–1953.

Fendell, F. E., Sprankle, M. L. & Dodson, D. S. 1966 Thin-flame theory for a fuel droplet in slow viscous flow. *J. Fluid Mech.* **26**, 267–280.

Feng, Z. G. & Michaelides, E. E. 1996 Unsteady heat transfer from a sphere at small Peclet numbers. *Trans. ASME* I: *J. Fluids Engng* **118**, 96–102.

Fuchs, N. A. 1959 *Evaporation and Droplet Growth in Gaseous Media*. Pergamon.

Godsave, G. A. E. 1953 Studies of the combustion of drops in a fuel spray: the burning of single drops of fuel. *Proc. Combust. Inst.* **4**, 818–830.

Gogos, G., Sadhal, S. S., Ayyaswamy, P. S. & Sundararajan, T. 1986 Thin-flame theory for the combustion of a moving liquid-drop. Effects due to variable density. *J. Fluid Mech.* **171**, 121–144.

Hermanns, M. 2006 High-order numerical methods applied to the analysis of transport phenomena in combustion. PhD thesis, Universidad Politécnica de Madrid, Madrid, Spain, pp. 45–77.

Hinch, E. J. 1993 The approach to steady state in Oseen flows. *J. Fluid Mech.* **256**, 601–604.

Jog, M. A., Ayyaswamy, P. S. & Cohen, I. M. 1996 Evaporation and combustion of slowly moving luiquid fuel droplets. *J. Fluid Mech.* **307**, 135–165.

Law, C. K. 1982 Recent advances in droplet vaporization and combustion. *Prog. Energy Combust. Sci.* **8**, 171–201.

Levich, V. G. 1962 *Physicochemical Hydrodynamics*, pp. 395–457. Prentice-Hall.

Ockendon, R. J. 1968 The unsteady motion of a small sphere in a viscous liquid. *J. Fluid Mech.* **34**, 229–239.

Oseen, C. W. 1910 Ueber die Stokes'sche formel, und über eine verwandte aufgave in der Hydrodynamik. *Ark. Mat. Astr. Fys.* **6**, 1–20.

Pozrikidis, C. 1997 Unsteady heat or mass transport from a suspended particle at low Péclet numbers. *J. Fluid Mech.* **334**, 111–133.

Proudman, I. & Pearson, J. R. A. 1957 Expansions of small Reynolds numbers for the flow past a sphere and a circular cylinder. *J. Fluid Mech.* **2**, 237–262.

Sadhal, S. S. & Ayyaswamy, P. S. 1983 Flow past a fluid drop with a large non-uniform radial velocity. *J. Fluid Mech.* **133**, 65–81.

Sano, T. 1981 Unsteady flow past a sphere at low Reynolds number. *J. Fluid Mech.* **112**, 433–441.

Sirignano, W. 1983 Fuel-droplet vaporization and spray combustion theory. *Prog. Energy Combust. Sci.* **9**, 299–322.

Sirignano, W. A. 1999 *Fluid Dynamics and Transport of Droplets and Sprays*, pp. 7–76. Cambridge University Press.

Spalding, D. B. 1953 The combustion of liquid fuels. *Proc. Combust. Inst.* **4**, 847–864.

Stokes, G. G. 1851 On the effect of internal friction of fluids on the motion of pendulums. *Trans. Camb. Phil. Soc.* **9**, 8–106.

Waldman, C. H. 1975 Theory of non-steady state droplet combustion. *Proc. Combust. Inst.* **5**, 429–442.

Wichman, I. S. & Baum, H. R. 1993 A solution procedure for low Reynolds number combustion problems under microgravity conditions. In *Heat Transfer in Microgravity* (ed. C. T. Avedisan & V. A. Arpaci, pp. 111–117. American Society of Mechanical Engineers.

Williams, A. 1973 Combustion of droplets of liquid fuels: a review. *Combust. Flame* **21**, 1–31.

Williams, F. A. 1965 *Combustion Theory*, pp. 47–57. Addison–Wesley.

Williams, F. A. 1985 *Combustion Theory*, 2nd edn, pp. 52–69. Addison-Wesley.